



Published in final edited form as:

Biochem Pharmacol. 2022 January ; 195: 114868. doi:10.1016/j.bcp.2021.114868.

Structure-activity studies of PTPRD phosphatase inhibitors identify a 7-cyclopentymethoxy illudalic acid analog candidate for development

Ian M. Henderson^{a,b}, Fanxun Zeng^c, Nazmul H. Bhuiyan^d, Dan Luo^d, Maria Martinez^{a,b}, Jane Smoake^{a,b}, Fangchao Bi^c, Chamani Perera^e, David Johnson^e, Thomas E. Prisinzano^{d,*}, Wei Wang^{c,*}, George R. Uhl^{a,b,f,g,h,*}

^aBiomedical Research Institute of New Mexico, Albuquerque, NM, United States

^bNew Mexico VA Healthcare System, Albuquerque, NM, United States

^cCollege of Pharmacy, University of Arizona, Tucson, AZ, United States

^dCollege of Pharmacy, University of Kentucky, Lexington, KY, United States

^eUniversity of Kansas, Lawrence, KS, United States

^fDepartments of Neurology, Neuroscience and Molecular Genetics and Microbiology, University of New Mexico, Albuquerque, NM, United States

^gDepartments of Neurology and Pharmacology, University of Maryland School of Medicine, Baltimore, MD, United States

^hVA Maryland Healthcare System, Baltimore, MD, United States

Abstract

Interest in development of potent, selective inhibitors of the phosphatase from the receptor type protein tyrosine phosphatase PTPRD as antiaddiction agents is supported by human genetics, mouse models and studies of our lead compound PTPRD phosphatase inhibitor, 7-butoxy illudalic acid analog **1** (7-BIA). We now report structure–activity relationships for almost 70 7-BIA-related compounds and results that nominate a 7- cyclopentyl methoxy analog as a candidate for further development. While efforts to design 7-BIA analogs with substitutions for other parts failed to yield potent inhibitors of PTPRD’s phosphatase, ten 7-position substituted analogs displayed greater potency at PTPRD than 7-BIA. Several were more selective for PTPRD vs the receptor type protein tyrosine phosphatases S, F and J or the nonreceptor type protein tyrosine phosphatase

*Corresponding authors at: University of Maryland School of Medicine and Maryland VA Healthcare System, Baltimore, MD, United States (G.R. Uhl). prisinzano@uky.edu (T.E. Prisinzano), wwang@pharmacy.arizona.edu (W. Wang), George.uhl@va.gov (G.R. Uhl). CRediT authorship contribution statement

Ian M. Henderson: Investigation, Analyses. **Fanxun Zeng:** Data curation, Investigation. **Nazmul H. Bhuiyan:** Data curation, Investigation. **Dan Luo:** Investigation. **Maria Martinez:** Data curation, Investigation. **Jane Smoake:** Investigation. **Fangchao Bi:** Investigation. **Chamani Perera:** Investigation. **David Johnson:** Conceptualization, Funding acquisition, Investigation, Analyses. **Thomas E. Prisinzano:** Conceptualization, Funding acquisition, Investigation, Supervision. **Wei Wang:** Conceptualization, Funding acquisition, Investigation, Supervision. **George R. Uhl:** Conceptualization, Supervision, Analyses, Product administration.

Declaration of Competing Interest

The authors declare that they have no known competing financial interests or personal relationships that could have appeared to influence the work reported in this paper.

N1 (PTPRS, PTPRF, PTPRJ or PTPN1/PTP1B), phosphatases at which 7-BIA displays activity. *In silico* studies aided design of novel analogs. A 7-position cyclopentyl methoxy substituted 7-BIA analog termed NHB1109 displayed 600–700 nM potencies in inhibiting PTPRD and PTPRS, improved selectivity vs PTPRS, PTPRF, PTPRJ or PTPN1/PTP1B phosphatases, no substantial potency at other protein tyrosine phosphatases screened, no significant potency at any of the targets of clinically-useful drugs identified in EUROFINS screens and significant oral bioavailability. Oral doses up to 200 mg/kg were well tolerated by mice, though higher doses resulted in reduced weight and apparent ileus without clear organ histopathology. NHB1109 provides a good candidate to advance to *in vivo* studies in addiction paradigms and toward human use to reduce reward from addictive substances.

Keywords

Receptor type protein tyrosine phosphatase; Cell adhesion molecule; Addiction; Drug reward; Opiates; Stimulants

1. Introduction

Development of safe and effective medications to prevent and treat substance use disorders (SUDs) is an urgent public health need. Current approaches to reducing abuse liability of prescribed opiates or stimulants are only modestly effective for many individuals. There are no Food and Drug Administration (FDA)-approved medications for cocaine or methamphetamine use disorders. Agonist-like, antagonist and other therapeutics for opiate use disorders provide benefits, but remain suboptimal for many [1]. A “fourth wave” of US drug overdose deaths now includes increasing numbers of individuals who use both opiates and stimulants [2]. Optimal addiction medications development portfolios should include new drugs that act at novel targets that are as well supported as possible, *a priori*, by human and other data.

Levels of tyrosine phosphorylation are common mechanisms by which functions of important cellular proteins can be regulated [3]. These phosphorylation levels are regulated by opposing actions of protein tyrosine kinases and protein tyrosine phosphatases, which catalyze phosphate addition to or removal from key tyrosine residues of these phosphoproteins, respectively [4,5]. Phosphatase catalytic sites display strong sequence conservation and preference for negative charges that can render them difficult to “drug” [3]. Nevertheless, phosphatase inhibitors have been developed with selectivities sufficient to advance to use in clinical trials, supporting the idea that such phosphatases are not “undruggable” [6].

The receptor type protein tyrosine phosphatase D (PTPRD) is now a strongly-supported target for antiaddiction medications based on human, mouse model and *in vitro* data [7]. Human genetic results [8] associate common variation in PTPRD with vulnerability to develop a substance use disorder (polysubstance [9–11], opiate use disorder [12], alcohol use disorder [13]), ability to quit (smoking [14,15], use of opiates [16] and use of alcohol when aided by an opiate antagonist [17]), rewarding responses to amphetamine administration [18,19], alcohol effects during the “first five” occasions for consumption [20]

and levels of expression of PTPRD messenger RNA (mRNA) in human postmortem cortex [21]. Mice or rats with reduced PTPRD expression or pharmacological PTPRD inhibition display reduced reward from stimulants and opiates in conditioned place preference and self administration assays [22,23].

PTPRD is a highly-expressed, largely-neuronal, substantially synaptic, single transmembrane protein that likely transduces signals from binding to extracellular ligands [24] to alter activity of its intracellular phosphatase [25]. Several PTPRD extracellular binding partners have been nominated include slit/trk, interleukin-1 receptor like and accessory proteins and synaptic adhesion-like molecules (SALMs) [26–30]. Substrates for PTPRD's phosphatase, identified by phosphoproteomic studies of proteins extracted from brains of wildtype vs PTPRD knockout mice and confirmatory studies, include proteins that regulate synaptic strength and maturation [31]. Neuronal processes of PTPRD-expressing neurons grow when their PTPRD makes homomeric bonds with PTPRD expressed by adjacent cells [32]. Ventral midbrain, striatal/accumbens, cortical, reticular thalamic and other circuits that express PTPRD mRNA in likely dopamine, acetylcholine, glutamate and gamma amino butyric acid (GABA) neurons [33] are likely to adapt differently when they express PTPRD at differing levels.

PTPRD is a member of a subfamily of receptor type protein tyrosine phosphatases that also includes PTPRS and PTPRF. Previous work found that illudalic acid analogs (Fig. 1) can inhibit PTPRF's phosphatase [34,35]. This work appears to support pseudo-irreversible inhibition of PTPRF's phosphatase by illudalic acid analogs, though no available crystallographic data supports this model [34,35].

Illudalic acid was originally isolated from *Clitocybe illudens*; a method for its synthesis has been reported [36,37]. Recently, we found that the butoxy analog 7-BIA (**1**) inhibits the ability of PTPRD's phosphatase to dephosphorylate the small molecule phosphatase substrate, *para*-nitrophenol phosphate (*p*-NPP), with good potency [22]. Additional work found that 7-BIA provided no apparent toxicities in mice which received either acute ascending doses or 2-week repeated doses up to 20 mg/kg [22]. Pretreating mice with 10–20 mg/kg doses of 7-BIA reduced cocaine reward in both self-administration and conditioned place preference assays [21,22]. 7-BIA displayed no significant activities in EUROFINS screens for targets of currently-licensed drugs [22,38], but it was active at the phosphatases from PTPRD and its two closest relatives, PTPRS and PTPRF [22,35].

Despite these interesting features, PTPRD has no reported *in vitro* small molecule SAR data. To improve understanding of the interactions of PTPRD and 7-BIA, as well as to identify routes to development of improved PTPRD phosphatase inhibitors as potential anti-addiction therapeutics, we now report synthesis and *in vitro* tests of activities of a series of novel illudalic acid congeners. To gain greater insight into the interactions of this class of PTPRD ligands, we investigate possible modes of binding to PTPRD's phosphatase using molecular docking *in silico*. We report identification of a 7-cyclopentylmethoxy analog that displays increased potency, selectivity, oral bioavailability and *in vivo* tolerability. This 7-cyclopentylmethoxy analog provides a good candidate for experimental animal anti-addiction studies and development toward use in humans.

2. Materials and methods

2.1. General

Reagents and solvents were purchased from Sigma-Aldrich (St. Louis, MO), Fisher Scientific (Waltham, MA), AmBeed (Arlington Heights, IL), and NetChem Inc. (New Brunswick, NJ). All reactions in nonaqueous solvents were conducted in flame-dried glassware under a positive pressure of argon and with magnetic stirring. All NMR spectra were obtained at 400 MHz for ^1H , 100 MHz for ^{13}C with internal standards of $(\text{CH}_3)_4\text{Si}$ (^1H , 0.00), CHCl_3 (^1H , 7.27; ^{13}C , 77.2 ppm), and MeOH (^1H , 3.34; ^{13}C , 49.86) for non-aqueous samples or H_2O (^1H , 4.80) unless mentioned otherwise. Elemental analyses were obtained from the Atlantic Microlab Inc., GA and are within 0.4%. Silica gel (60 Å, 0.040–0.063 mm) was used for flash chromatography in an ISCO combiflash instrument. The purity of all final compounds was determined to be >95% by analytical high-performance liquid chromatography (HPLC) analysis and/or combustion analysis.

2.2. Experimental details for the synthesis of 66 and related analogs

6-Benzyloxy-7-methoxy-3H-indene-4-carboxylic acid methyl ester (63).—A mixture of 6-hydroxy-7-methoxy-1-oxo-indan-4-carboxylic acid methyl ester (5.00 g, 21.2 mmol) and K_2CO_3 (4.40 g, 32 mmol) in CH_3CN (80 mL) was stirred for 30 min at room temperature. Benzyl bromide (4.4 g, 25.5 mmol) was added and the combined mixture was heated at reflux for 14 h. The mixture was poured into H_2O (50 mL) and extracted with EtOAc (100 mL). The organic layer was collected, washed with H_2O (2×50 mL) and brine (30 mL), dried (Na_2SO_4), and concentrated under reduced pressure. The resulting solid was dissolved in MeOH (100 mL), cooled to 0 °C, and treated with NaBH_4 (1.09 g, 29 mmol). The reaction mixture was allowed to reach room temperature and stirred for 2 h. After removal of the solvent, 2 N aqueous HCl (50 mL) was added slowly. This aqueous layer was then extracted with EtOAc (3×80 mL). The combined extract was dried (Na_2SO_4) and evaporated to dryness under reduced pressure. Anhydrous toluene (10 mL) was then added to the resulting solid and removed under reduced pressure 3 times. The solid was dissolved in toluene (100 mL) followed by the addition of TsOH· H_2O (0.217 g, 1.25 mmol). The reaction mixture was heated at 80 °C for 20 min, cooled to room temperature, diluted with EtOAc (100 mL), and washed with H_2O (50 mL) and brine (30 mL). The organic layer was dried over Na_2SO_4 , evaporated to dryness under reduced pressure, and subjected to flash column chromatography (10% EtOAc in hexane) to afford **63** (6.100 g, 78% over 3 steps): ^1H NMR (400 MHz, CDCl_3) δ 7.53 (s, 1H), 7.48–7.32 (m, 5H), 7.01 (m, 1H), 6.58 (m, 1H), 5.15 (s, 2H), 3.99 (s, 3H), 3.90 (s, 3H), 3.69 (m, 2H); ^{13}C NMR (100 MHz, CDCl_3) 166.9, 149.9, 146.8, 140.8, 138.8, 136.9, 135.5, 128.5, 128.0, 127.5, 127.5, 120.5, 113.0, 71.5, 61.2, 51.8, 41.0.

1,2,6-Trihydroxy-7-methoxy-indan-4-carboxylic acid methyl ester (64).—A 250 mL flask was charged with AD-mix- α (28 g), H_2O (45 mL), and *t*-BuOH (45 mL). The mixture was cooled to 0 °C followed by the addition of methanesulfonamide (2.00 g, 21 mmol) and **63** (5.70 g, 18.4 mmol). The reaction mixture was warmed to room temperature and stirred for 16 h. Upon disappearance of the starting material, sodium sulfite (29.50 g) was added and the reaction mixture was stirred for additional 30 min. The mixture was

diluted by the addition of H₂O (50 mL) and EtOAc (100 mL). The organic layer was collected, and the aqueous layer was extracted with EtOAc (3 × 100 mL). The combined organic layers were washed with 2 N KOH (40 mL) and brine (50 mL), dried (Na₂SO₄), and concentrated under reduced pressure. The resulting solid was dissolved in MeOH (100 mL), charged with Pd/C (5% Pd on charcoal, 1.00 g) and a magnetic stirrer. A balloon filled with H₂ gas was connected to the reaction flask through a rubber septum and vigorously stirred for 14 h. The mixture was filtered through a pad of celite and concentrated under reduced pressure. The residue was then subjected to a column chromatography using EtOAc as the eluent to afford **64** (4.20 g, 81% overall 2 steps): ¹H NMR (400 MHz, CD₃OD) δ 7.39 (s, 1H), 5.00 (d, *J* = 8.0 Hz, 1H), 4.26–4.21 (m, 1H), 3.99 (s, 3H), 3.81 (s, 3H), 3.41–3.34 (m, 1H), 3.04–2.98 (m, 1H); ¹³C NMR (100 MHz, CD₃OD) 166.9, 149.3, 147.9, 136.2, 134.8, 121.1, 118.5, 72.8, 71.6, 59.9, 50.8, 37.9.

6-Cyclopentylmethoxy-1,2-dihydroxy-7-methoxy-indan-4-carboxylic acid methyl ester (65).—A mixture of **64** (0.300 g, 1.2 mmol) and K₂CO₃ (0.196 g, 1.30 mmol) in DMF (10 mL) was stirred for 30 min. (Bromomethyl)cyclopentane (0.212 g, 1.30 mmol) was added and the reaction was heated at 80 °C for 6 h. The reaction mixture was then partitioned between EtOAc (30 mL) and H₂O (15 mL). The organic layer was collected and the aqueous layer was extracted with EtOAc (2 × 20 mL). The combined organic extracts were washed with brine (15 mL), dried (Na₂SO₄), and concentrated under reduced pressure. The resulting material was subjected to a flash chromatography using hexane:EtOAc (1:1) as eluent to afford **65** (0.320 g, 81%): ¹H NMR (400 MHz, CDCl₃) δ 7.47 (s, 1H), 5.13 (m, 1H), 4.42 (m, 1H), 4.01 (s, 3H), 3.85–3.83 (m, 5H), 3.35–3.19 (m, 3H), 1.37 (m, 1H), 1.85 (d, *J* = 4.0 Hz, 1H), 1.84–1.82 (m, 2H), 1.63–1.58 (m, 4H), 1.37–1.33 (m, 2H); ¹³C NMR (100 MHz, CDCl₃) δ 166.7, 150.4, 150.2, 137.1, 135.1, 121.5, 116.3, 73.4, 72.8, 72.6, 61.0, 51.8, 39.2, 39.1, 29.5, 25.4.

7-Cyclopentylmethoxy-3-hydroxy-6-methoxy-1-oxo-isochroman-5-carbaldehyde (58).—A mixture of **65** (0.600 g, 1.8 mmol), methanolic 2 N KOH (3 mL) was stirred at 75 °C for 2 h. After removal of the solvent under reduced pressure, aqueous 2 N HCl was added until the pH lowered to 1–2. The aqueous mixture was then extracted with EtOAc (5 × 15 mL). The combined organic extracts were dried (Na₂SO₄) and concentrated under reduced pressure. The solid obtained (0.500 g) was dissolved in 50% aqueous solution of dioxane (5 mL), treated with NaIO₄ (0.500 g, 2.3 mmol) and the mixture was stirred at room temperature for 2.5 h. The mixture was partitioned between EtOAc (10 mL) and H₂O (5 mL) and organic layer was collected. The aqueous layer was extracted with EtOAc (5 × 20 mL). The combined organic extracts were washed with brine (15 mL), dried (Na₂SO₄), and evaporated to dryness under reduced pressure. CH₂Cl₂ (5 mL) was added to the residue and the mixture was filtered. The CH₂Cl₂ solution was concentrated under reduced pressure, and the solid obtained was washed with dry Et₂O: hexane (1:1, 2 × 3 mL) to afford **58** (0.340 g, 68% over 2 steps): ¹H NMR (400 MHz, CDCl₃) δ 10.51 (s, 1H), 7.84 (s, 1H), 5.89 (m, 1H), 4.09 (s, 3H), 3.99–3.94 (m, 3H), 3.64–3.44 (m, 2H), 2.45–2.42 (m, 1H), 1.89–1.85 (m, 2H), 1.68–1.57 (m, 4H), 1.39–1.34 (m, 2H); ¹³C NMR (100 MHz, CDCl₃) δ 191.8, 164.5, 158.3, 151.2, 130.4, 126.9, 120.4, 118.5, 95.5, 73.4, 62.2, 38.9, 30.7, 29.6, 25.4; Elemental analysis calculated (%) for C₁₇H₂₀O₆: C 63.74, H 6.29; found: C 63.49, H 6.37.

The following compounds were synthesized by routes similar to that described for **58**: **27**, **28**, **30**, **37**, **38**, **40**, **41**, **42**, **44**, **45**, **46**, **47**, **48**, **50**, **51**, **55**, **56**, **57**, **59**, **60**, **61**.

7-(Benzyloxy)-3-hydroxy-6-methoxy-1-oxoisochromane-5-carbaldehyde (27).—

¹H NMR (400 MHz, DMSO-*d*₆) δ 10.37 (s, 1H), 7.86 (s, 1H), 7.74 (d, *J* = 5.5 Hz, 1H), 7.51–7.44 (m, 2H), 7.40 (t, *J* = 7.6 Hz, 2H), 7.36–7.29 (m, 1H), 5.74 (q, *J* = 4.6 Hz, 1H), 5.27 (s, 2H), 3.99 (s, 3H), 3.38–3.31 (m, 1H), 3.27–3.22 (m, 1H); ¹³C NMR (100 MHz, DMSO-*d*₆) δ 192.35, 163.60, 157.60, 150.66, 136.74, 131.34, 129.02, 128.55, 128.11, 127.58, 121.47, 119.11, 95.76, 70.81, 62.50, 31.51; HRMS (ESI): C₁₈H₁₇O₆⁺ (M + H): 329.1020, found: 329.1021.

3-Hydroxy-6-methoxy-7-((4-methylbenzyl)oxy)-1-oxoisochromane-5-carbaldehyde (28).—

¹H NMR (400 MHz, CDCl₃) δ 10.51 (s, 1H), 7.96 (s, 1H), 7.33 (d, *J* = 7.6 Hz, 2H), 7.20 (d, *J* = 7.6 Hz, 2H), 5.90 (t, *J* = 3.8 Hz, 1H), 5.13 (s, 2H), 4.52 (br s, 1H), 4.06 (s, 3H), 3.67–3.57 (m, 1H), 3.52–3.43 (m, 1H), 2.36 (s, 3H); ¹³C NMR (100 MHz, CDCl₃) δ 191.70, 163.91, 158.55, 150.75, 138.34, 132.50, 130.77, 129.42, 127.77, 127.08, 120.51, 119.31, 95.31, 71.21, 62.30, 30.72, 21.21; HRMS (ESI): C₁₉H₁₈O₆Na⁺ (M + Na): 365.0996, found: 365.0998.

3-Hydroxy-6-methoxy-7-((3-methoxybenzyl)oxy)-1-oxoisochromane-5-carbaldehyde (30).—

¹H NMR (400 MHz, Acetone-*d*₆) δ 10.49 (s, 1H), 7.97 (s, 1H), 7.52 (dd, *J* = 7.6, 1.8 Hz, 1H), 7.35 (td, *J* = 8.0, 1.8 Hz, 1H), 7.07 (d, *J* = 8.4 Hz, 1H), 6.99 (t, *J* = 7.4 Hz, 1H), 6.67 (d, *J* = 6.8 Hz, 1H), 5.88–5.82 (m, 1H), 5.29 (s, 2H), 4.09 (s, 3H), 3.90 (s, 3H), 3.46–3.41 (m, 2H); ¹³C NMR (100 MHz, Acetone-*d*₆) δ 191.37, 162.81, 157.87, 157.48, 150.78, 130.78, 129.76, 129.39, 127.34, 124.24, 121.53, 120.44, 118.87, 110.71, 95.26, 65.99, 61.62, 55.01, 31.14; HRMS (ESI): C₁₉H₁₈O₇ Na⁺ (M + Na): 381.0945, found: 381.0945.

7-((4-Bromobenzyl)oxy)-3-hydroxy-6-methoxy-1-oxoisochromane-5-carbaldehyde (37).—

¹H NMR (400 MHz, CDCl₃) δ 10.51 (s, 1H), 7.92 (s, 1H), 7.53 (d, *J* = 8.0 Hz, 2H), 7.32 (d, *J* = 8.0 Hz, 2H), 5.90 (t, *J* = 3.6 Hz, 1H), 5.12 (s, 2H), 4.60 (br s, 1H), 4.06 (s, 3H), 3.63 (dd, *J* = 18.0, 3.6 Hz, 1H), 3.47 (dd, *J* = 18.0, 3.6 Hz, 1H); ¹³C NMR (100 MHz, CDCl₃) δ 191.54, 163.89, 158.47, 150.51, 134.52, 131.95, 131.16, 129.25, 127.24, 122.51, 120.63, 119.23, 95.32, 70.54, 62.38, 30.71; HRMS (ESI): C₁₈H₁₅⁷⁹BrO₆Na⁺ (M + Na): 428.9944, found: 428.9948; C₁₈H₁₅⁸¹BrO₆Na⁺ (M + Na): 430.9924, found: 430.9926.

7-((2,4-Dichlorobenzyl)oxy)-3-hydroxy-6-methoxy-1-oxoisochromane-5-carbaldehyde (38).—

¹H NMR (400 MHz, Acetone-*d*₆) δ 10.50 (s, 1H), 7.96 (s, 1H), 7.79–7.73 (m, 1H), 7.62–7.57 (m, 1H), 7.51–7.47 (m, 1H), 5.88 (s, 1H), 5.39 (s, 2H), 5.29 (s, 1H), 4.10 (s, 3H), 3.48–3.44 (m, 2H); ¹³C NMR (100 MHz, Acetone-*d*₆) δ 191.25, 162.69, 157.68, 150.45, 142.91, 134.51, 133.11, 131.42, 131.12, 129.18, 127.63, 121.70, 118.85, 117.37, 101.33, 67.81, 61.93, 31.15; HRMS (ESI): C₁₈H₁₄³⁵Cl₂O₆Na⁺ (M + Na): 419.0060, found: 419.0066; C₁₈H₁₄³⁵Cl³⁷ClO₆Na⁺ (M + Na): 421.0030, found: 421.0035; C₁₈H₁₄³⁷Cl₂O₆Na⁺ (M + Na): 423.0001, found: 423.0005.

3-Hydroxy-6-methoxy-1-oxo-7-((4-phenoxybenzyl)oxy)isochromane-5-carbaldehyde (40).—¹H NMR (400 MHz, CDCl₃) δ 10.51 (s, 1H), 7.96 (s, 1H), 7.40 (d, *J* = 8.0 Hz, 2H), 7.34 (t, *J* = 7.8 Hz, 2H), 7.12 (t, *J* = 7.4 Hz, 1H), 7.05–6.99 (m, 4H), 5.91 (t, *J* = 3.8 Hz, 1H), 5.13 (s, 2H), 4.65 (br s, 1H), 4.07 (s, 3H), 3.67–3.59 (m, 1H), 3.52–3.43 (m, 1H); ¹³C NMR (100 MHz, CDCl₃) δ 191.65, 163.97, 158.55, 157.68, 156.66, 150.69, 130.95, 130.08, 129.82, 129.40, 127.16, 123.65, 120.58, 119.34, 119.24, 118.71, 95.34, 70.91, 62.34, 30.73; HRMS (ESI): C₂₄H₂₀O₇Na⁺ (M + Na): 443.1101, found: 443.1100.

7-((4-(4-Fluorophenoxy)benzyl)oxy)-3-hydroxy-6-methoxy-1-oxoisochromane-5-carbaldehyde (41).—¹H NMR (400 MHz, Acetone-*d*₆) δ 10.49 (s, 1H), 7.93 (s, 1H), 7.58 (d, *J* = 8.4 Hz, 2H), 7.16 (t, *J* = 8.4 Hz, 2H), 7.10–7.05 (m, 2H), 7.03 (d, *J* = 8.4 Hz, 2H), 6.68 (d, *J* = 5.6 Hz, 1H), 5.87 (q, *J* = 4.5 Hz, 1H), 5.28 (s, 2H), 4.10 (s, 3H), 3.44 (d, *J* = 4.1 Hz, 2H); ¹³C NMR (100 MHz, Acetone-*d*₆) δ 191.33, 162.80, 158.92 (d, ¹JCF = 238.9 Hz), 157.86, 157.82, 152.82 (d, ⁴JCF = 2.3 Hz), 150.69, 131.27, 130.95, 129.78, 127.37, 121.51, 120.94 (d, ³JCH = 8.4 Hz), 118.88, 118.03, 116.35 (d, ²JCF = 23.2 Hz), 95.26, 70.41, 61.76, 31.13; ¹⁹F NMR (376 MHz, Acetone-*d*₆) δ –121.21––121.29 (m, 1F); HRMS (ESI): C₂₄H₁₉FO₇Na⁺ (M + Na): 461.1007, found: 461.1013.

3-Hydroxy-6-methoxy-7-((5-methylthiophen-2-yl)methoxy)-1-oxoisochromane-5-carbaldehyde (42).—¹H NMR (400 MHz, CDCl₃) δ 10.50 (s, 1H), 7.96 (s, 1H), 6.93 (d, *J* = 3.6 Hz, 1H), 6.64 (d, *J* = 3.6 Hz, 1H), 5.89 (t, *J* = 3.8 Hz, 1H), 5.25 (s, 2H), 4.22 (s, 1H), 4.08 (s, 3H), 3.62 (dd, *J* = 18.0, 3.8 Hz, 1H), 3.47 (dd, *J* = 18.0, 3.8 Hz, 1H), 2.47 (s, 3H); ¹³C NMR (100 MHz, CDCl₃) δ 191.65, 163.66, 158.65, 150.10, 141.80, 135.09, 130.98, 127.89, 127.09, 124.96, 120.39, 119.58, 95.22, 66.24, 62.38, 30.71, 15.42; HRMS (ESI): C₁₇H₁₆O₆SNa⁺ (M + Na): 371.0560, found: 371.0561.

3-Hydroxy-6-methoxy-7-(naphthalen-2-ylmethoxy)-1-oxoisochromane-5-carbaldehyde (44).—¹H NMR (400 MHz, CDCl₃) δ 10.53 (s, 1H), 8.03 (s, 1H), 7.92–7.82 (m, 4H), 7.58–7.47 (m, 3H), 5.89 (s, 1H), 5.33 (s, 2H), 4.09 (s, 3H), 3.66–3.44 (m, 2H); ¹³C NMR (100 MHz, CDCl₃) δ 191.61, 163.50, 158.54, 150.78, 133.21, 133.18, 132.90, 130.77, 128.68, 128.00, 127.75, 127.15, 126.88, 126.48, 126.44, 125.22, 120.64, 119.34, 95.17, 71.47, 62.38, 30.71; HRMS (ESI): C₂₂H₁₈O₆Na⁺ (M + Na): 401.0996, found: 401.0996.

3-Hydroxy-6-methoxy-1-oxo-7-phenethoxyisochromane-5-carbaldehyde (45).—¹H NMR (400 MHz, CDCl₃) δ 10.48 (s, 1H), 7.85 (s, 1H), 7.37–7.28 (m, 3H), 7.27–7.19 (m, 2H), 5.88 (t, *J* = 3.8 Hz, 1H), 4.33 (t, *J* = 6.6 Hz, 2H), 3.89 (s, 3H), 3.60 (d, *J* = 17.6 Hz, 1H), 3.45 (d, *J* = 17.6 Hz, 1H), 3.17 (t, *J* = 6.6 Hz, 2H); ¹³C NMR (100 MHz, CDCl₃) δ 191.66, 163.81, 158.27, 150.88, 137.60, 130.53, 128.84, 128.58, 127.04, 126.74, 120.54, 118.69, 95.26, 69.84, 62.17, 35.51, 30.68; HRMS (ESI): C₁₉H₁₈O₆Na⁺ (M + Na): 365.0996, found: 365.0991.

3-Hydroxy-6-methoxy-1-oxo-7-(2-pyrrol-1-yl-ethoxy)isochromane-5-carbaldehyde (46).—¹H NMR (400 MHz, CDCl₃) δ 10.48 (s, 1H), 7.82 (s, 1H), 6.75 (m, 2H), 6.15 (m, 2H), 5.88 (m, 1H), 4.35 (m, 4H), 3.90 (s, 3H), 3.59–3.45 (m, 3H); ¹³C NMR (100 MHz, CDCl₃) δ 191.8, 164.0, 158.6, 150.9, 131.3,

127.3, 120.8, 120.7, 118.8, 108.8, 95.4, 69.0, 62.3, 48.6, 30.7; Elemental analysis calculated (%) for $C_{17}H_{17}NO_6 \cdot 0.25 H_2O$: C 60.80, H 5.25, N 4.17; found: C 60.50, H 5.19, N 4.19.

3-Hydroxy-6-methoxy-1-oxo-7-(3-phenylpropoxy)isochromane-5-carbaldehyde (47).— 1H NMR (400 MHz, $CDCl_3$) δ 10.52 (s, 1H), 7.82 (s, 1H), 7.29 (t, $J = 7.4$ Hz, 2H), 7.24–7.16 (m, 3H), 5.90 (t, $J = 3.6$ Hz, 1H), 4.13–3.99 (m, 5H), 3.68–3.40 (m, 2H), 2.83 (t, $J = 7.6$ Hz, 2H), 2.19 (p, $J = 6.7$ Hz, 2H); ^{13}C NMR (100 MHz, $CDCl_3$) δ 191.72, 163.97, 158.28, 151.05, 140.81, 130.46, 128.55, 128.37, 127.01, 126.17, 120.55, 118.69, 95.31, 68.33, 62.25, 32.17, 30.70, 30.64; HRMS (ESI): $C_{20}H_{20}O_6Na^+$ (M + Na): 379.1152, found: 379.1156.

7-(4-(4-Chlorophenyl)butoxy)-3-hydroxy-6-methoxy-1-oxoisochromane-5-carbaldehyde (48).— 1H NMR (400 MHz, $CDCl_3$) δ 10.50 (s, 1H), 7.83 (s, 1H), 7.24 (d, $J = 8.4$ Hz, 2H), 7.11 (d, $J = 8.4$ Hz, 2H), 5.90 (s, 1H), 4.36 (s, 1H), 4.09 (t, $J = 6.0$ Hz, 2H), 4.04 (s, 3H), 3.61 (dd, $J = 18.0, 3.8$ Hz, 1H), 3.46 (dd, $J = 18.0, 3.8$ Hz, 1H), 2.67 (t, $J = 7.2$ Hz, 2H), 1.92–1.76 (m, 4H); ^{13}C NMR (100 MHz, $CDCl_3$) δ 191.67, 163.86, 158.26, 151.04, 140.17, 131.64, 130.40, 129.68, 128.48, 127.01, 120.57, 118.64, 95.27, 68.99, 62.22, 34.74, 30.68, 28.45, 27.68; HRMS (ESI): $C_{21}H_{21}^{35}ClO_6Na^+$ (M + Na): 427.0919, found: 427.0923; $C_{21}H_{21}^{37}ClO_6Na^+$ (M + Na): 429.0890, found: 429.0895.

3-Hydroxy-7-(isopentyloxy)-6-methoxy-1-oxoisochromane-5-carbaldehyde (50).— 1H NMR (400 MHz, $CDCl_3$) δ 10.51 (s, 1H), 7.85 (s, 1H), 5.90 (t, $J = 3.8$ Hz, 1H), 4.46 (br s, 1H), 4.10 (t, $J = 6.6$ Hz, 2H), 4.07 (s, 3H), 3.61 (dd, $J = 18.0, 3.8$ Hz, 1H), 3.47 (dd, $J = 18.0, 3.8$ Hz, 1H), 1.91–1.79 (m, 1H), 1.75 (q, $J = 6.7$ Hz, 2H), 0.98 (d, $J = 6.4$ Hz, 6H); ^{13}C NMR (100 MHz, $CDCl_3$) δ 191.77, 164.01, 158.31, 151.17, 130.27, 126.95, 120.50, 118.57, 95.31, 67.77, 62.17, 37.75, 30.69, 25.13, 22.50, 22.46; HRMS (ESI): $C_{16}H_{20}O_6Na^+$ (M + Na): 331.1152, found: 331.1151.

3-Hydroxy-6-methoxy-7-(3-methyl-but-2-enyloxy)-1-oxo-isochroman-5-carbaldehyde (51).— 1H NMR (400 MHz, $CDCl_3$) δ 10.54 (s, 1H), 7.87 (s, 1H), 5.88 (m, 1H), 5.50–5.46 (m, 1H), 4.64 (m, 2H), 4.07 (s, 3H), 3.64–3.45 (m, 3H), 1.80 (s, 3H), 1.79 (s, 3H); ^{13}C NMR (100 MHz, $CDCl_3$) δ 191.8, 164.0, 158.6, 150.9, 139.4, 130.4, 127.0, 120.5, 119.2, 118.5, 95.3, 66.1, 62.2, 30.7, 25.8, 18.3; Elemental analysis calculated (%) for $C_{16}H_{18}O_6$: C 62.74, H 5.92; found: C 62.70, H 5.94.

3-Hydroxy-6-methoxy-1-oxo-7-(4,4,4-trifluorobutoxy)isochromane-5-carbaldehyde (55).— 1H NMR (400 MHz, $CDCl_3$) δ 10.55 (s, 1H), 7.89 (s, 1H), 5.97–5.92 (m, 1H), 4.20 (t, $J = 6.0$ Hz, 2H), 4.01–3.95 (m, 1H), 3.68 (dd, $J = 18.0, 3.8$ Hz, 1H), 3.52 (dd, $J = 18.0, 3.8$ Hz, 1H), 2.45–2.30 (m, 2H), 2.24–2.14 (m, 2H); ^{13}C NMR (100 MHz, $CDCl_3$) δ 191.51, 163.46, 158.27, 150.74, 130.87, 127.28, 126.86 (q, $^1J_{CF} = 274.5$ Hz), 120.82, 118.79, 95.18, 67.56, 62.37, 30.74 (q, $^2J_{CF} = 29.4$ Hz) 30.68, 22.14 (q, $^3J_{CF} = 3.0$ Hz); ^{19}F NMR (376 MHz, $CDCl_3$) δ –66.29 (t, $J = 10.8$ Hz); HRMS (ESI): $C_{15}H_{15}F_3O_6Na^+$ (M + Na): 371.0713, found: 371.0705.

7-Cyclopropylmethoxy-3-hydroxy-6-methoxy-1-oxo-isochroman-5-carbaldehyde (56).— 1H NMR (400 MHz, $CDCl_3$) δ 10.52 (s, 1H), 7.82 (s, 1H),

5.88 (m, 1H), 4.12 (s, 3H), 3.93 (m, 2H), 3.62–3.48 (m, 2H), 3.10 (s, 1H), 1.32–1.27 (m, 1H), 0.68–0.65 (m, 2H), 0.38–0.35 (m, 2H); ^{13}C NMR (100 MHz, CDCl_3) δ 191.8, 164.0, 158.6, 151.0, 130.4, 127.0, 120.5, 119.0, 95.3, 74.1, 62.2, 43.4, 30.7, 10.2, 3.3; Elemental analysis calculated (%) for $\text{C}_{15}\text{H}_{16}\text{O}_6 \cdot \text{H}_2\text{O}$: C 58.06, H 5.85; found: C 58.02, H 6.00.

7-Cyclobutylmethoxy-3-hydroxy-6-methoxy-1-oxo-isochroman-5-carbaldehyde (57).— ^1H NMR (400 MHz, CDCl_3) δ 10.52 (s, 1H), 7.85 (s, 1H), 5.88 (m, 1H), 4.07 (s, 3H), 4.03 (m, 2H), 3.99–3.88 (m, 1H), 3.62–3.46 (m, 1H), 2.87–2.81 (m, 1H), 2.15 (m, 2H), 1.96–1.87 (m, 4H); ^{13}C NMR (100 MHz, CDCl_3) δ 191.8, 164.0, 158.3, 151.2, 130.3, 126.9, 120.5, 118.7, 95.3, 73.2, 62.1, 34.3, 30.7, 29.7, 24.9, 18.5; Elemental analysis calculated (%) for $\text{C}_{16}\text{H}_{18}\text{O}_6$: C 62.74, H 5.92; found: C 62.50, H 5.88.

7-Cyclohexylmethoxy-3-hydroxy-6-methoxy-1-oxo-isochroman-5-carbaldehyde (59).— ^1H NMR (400 MHz, CDCl_3) δ 10.52 (s, 1H), 7.85 (s, 1H), 5.88 (m, 1H), 4.07 (s, 3H), 3.89–3.86 (m, 2H), 3.65–3.45 (m, 2H), 2.91–2.70 (m, 6H), 1.37–1.06 (m, 5H); ^{13}C NMR (100 MHz, CDCl_3) δ 191.8, 164.0, 158.3, 151.2, 130.3, 126.9, 120.5, 118.7, 95.3, 73.2, 62.1, 34.3, 30.7, 29.7, 24.9, 18.5; Elemental analysis calculated (%) for $\text{C}_{18}\text{H}_{22}\text{O}_6 \cdot 0.25 \text{H}_2\text{O}$: C 63.80, H 6.69; found: C 63.62, H 6.66.

7-Cycloheptylmethoxy-3-hydroxy-6-methoxy-1-oxo-isochroman-5-carbaldehyde (60).— ^1H NMR (400 MHz, CDCl_3) δ 10.52 (s, 1H), 7.84 (s, 1H), 5.92 (m, 1H), 4.69 (s, 1H), 4.09 (s, 3H), 4.03 (m, 2H), 3.87–3.84 (m, 2H), 3.65–3.45 (m, 2H), 2.09–2.05 (m, 1H), 1.89–1.85 (m, 2H), 1.73–1.35 (m, 10H); ^{13}C NMR (100 MHz, CDCl_3) δ 191.9, 164.3, 158.3, 151.3, 130.3, 126.9, 120.4, 118.5, 95.4, 74.7, 62.3, 39.0, 31.1, 30.7, 28.6, 26.4.

7-Bicyclo[1.1.1]pentanylmethoxy-3-hydroxy-6-methoxy-1-oxo-isochroman-5-carbaldehyde (61).— ^1H NMR (400 MHz, CDCl_3) δ 10.52 (s, 1H), 7.81 (s, 1H), 5.87 (m, 1H), 4.11 (s, 3H), 4.03 (s, 2H), 3.64–3.44 (m, 2H), 2.58 (s, 1H), 1.87 (s, 6H); ^{13}C NMR (100 MHz, CDCl_3) δ 191.8, 164.1, 158.2, 151.0, 130.5, 126.9, 120.3, 118.7, 95.4, 69.3, 62.1, 49.9, 42.7, 30.7, 28.7; Elemental analysis calculated (%) for $\text{C}_{17}\text{H}_{18}\text{O}_6$: C 64.14, H 5.70; found: C 63.91, H 5.65.

2.3. Experimental details for the synthesis of 52

1,2-Dihydroxy-7-methoxy-6-trifluoromethanesulfonyloxy-indan-4-carboxylic acid methyl ester (66).—A solution of **64** (0.350 g, 1.4 mmol) in CH_2Cl_2 (15 mL) was cooled to 0 °C and Et_3N (0.153 g, 1.5 mmol) and PhNTf_2 (0.540 g, 1.5 mmol) were slowly added. The reaction mixture was allowed to reach room temperature and stirred for 2 h. The reaction mixture was then diluted with CH_2Cl_2 (10 mL) and quenched by the addition of aqueous 1 M HCl (10 mL). The organic layer was collected, and the aqueous layer was extracted with CH_2Cl_2 (2 × 20 mL). The organic extracts were combined, washed with brine (20 mL), dried over Na_2SO_4 , and concentrated under reduced pressure. The resulting residue was subjected to a flash chromatography using hexane:EtOAc (1:1) as eluent to afford **66** (0.410 g, 77%): ^1H NMR (400 MHz, CDCl_3) δ 7.81 (s, 1H), 5.22 (t, $J = 8.0$ Hz, 1H), 4.51 (m, 1H), 4.15 (s, 3H), 3.87 (s, 3H), 3.50 (m, 1H), 3.29 (m, 1H), 3.09 (d, $J = 8.0$ Hz,

1H), 2.69 (s, 1H); ¹³C NMR (100 MHz, CDCl₃) δ 165.1, 153.2, 146.3, 139.8, 134.5, 129.6, 125.2, 127.2–117.0 (m), 73.1, 72.6, 61.3, 52.2, 39.1.

1,2-Dihydroxy-7-methoxy-6-pent-1-enyl-indan-4-carboxylic acid methyl ester (67).—A flame dried Biotage™ microwave vial (20 mL) was charged with **66** (0.200 g, 0.52 mmol), *trans*-1-penten-1-ylboronic acid pinacol ester (0.152 g, 0.78 mmol), Na₂CO₃ (0.06 g, 0.56 mmol), and Pd(PPh₃)₄ (0.03 g, 0.026 mmol). The vial was capped, kept under vacuum for 20 min, and purged with argon. Priorly sonicated (10 min) H₂O (1 mL) and toluene (2 mL) were added to the reaction vial. The reaction mixture was heated to 90 °C and stirred for 6 h. After cooling to room temperature, reaction mixture was partitioned between EtOAc (15 mL) and H₂O (8 mL), and the organic layer was collected. The aqueous layer was extracted with EtOAc (3 × 15 mL), and the combined organic layer was washed with brine (10 mL), dried over Na₂SO₄, and concentrated under reduced pressure. The residue was then subjected to flash column chromatography using hexane:EtOAc (3:1) as eluent to obtain **67** (0.124 g, 78%): ¹H NMR (400 MHz, CDCl₃) δ 8.04 (s, 1H), 6.55 (m, 1H), 6.25 (m, 1H), 5.14 (m, 1H), 4.43 (m, 1H), 3.90 (s, 3H), 3.85 (s, 3H), 3.41–3.23 (m, 3H), 2.20 (m, 3H), 1.51 (m, 2H), 0.94 (m, 3H); ¹³C NMR (100 MHz, CDCl₃) δ 166.7, 158.1, 144.0, 134.4, 133.3, 130.2, 130.1, 123.3, 122.6, 73.0, 72.6, 61.3, 51.8, 39.5, 24.8, 22.4, 13.7.

3-Hydroxy-6-methoxy-1-oxo-7-pentyl-isochroman-5-carbaldehyde (52).—A methanolic solution of 2 N KOH (0.35 mL) was added to a solution of **67** (0.110 g, 0.36 mmol) in MeOH (0.2 mL). The reaction mixture was heated to 75 °C and stirred for 2 h. The solvent was removed under reduced pressure, and the residue was acidified to pH 1–2 by the addition of aqueous 2 N HCl and extracted with EtOAc (5 × 10 mL). The combined organic layer was dried (Na₂SO₄) and then evaporated to dryness under reduced pressure. The residue was dissolved in MeOH (1 mL), charged with Pd/C (20 mg, 5% metal loaded on charcoal), and stirred for 10 h under an atmosphere of hydrogen gas. The reaction was filtered through a pad of celite, washed with EtOAc, and the solvent was removed under reduced pressure. The solid obtained (25 mg) was dissolved in 50% aqueous solution of dioxane (2 mL) and then treated with NaIO₄ (0.022 g, 0.1 mmol). The mixture was stirred for 2 h at room temperature, partitioned between EtOAc (5 mL) and H₂O (3 mL) and the organic layer was collected. The aqueous layer was then extracted with EtOAc (5 × 5 mL). The combined organic extracts were washed with brine (5 mL), dried (Na₂SO₄), and evaporated to dryness under reduced pressure. CH₂Cl₂ (5 mL) was added to the residue and the mixture was filtered. The CH₂Cl₂ solution was concentrated under reduced pressure, and the solid obtained was washed with dry Et₂O (2 × 2 mL) to afford **52** (0.015 g, 14% over 3 steps): ¹H NMR (400 MHz, CDCl₃) δ 10.48 (s, 1H), 8.24 (s, 1H), 5.91 (m, 1H), 3.91 (s, 3H), 3.72–3.48 (m, 3H), 2.68 (t, *J* = 8.0 Hz, 2H), 1.67 (m, 2H), 1.35 (m, 4H), 0.90 (m, 3H); ¹³C NMR (100 MHz, CDCl₃) 191.7, 167.3, 164.1, 137.3, 137.1, 136.6, 126.9, 121.4, 95.2, 64.3, 31.7, 31.1, 29.8, 28.9, 22.4, 14.0; Elemental analysis calculated (%) for C₁₆H₂₀O₅: C 65.74, H 6.90; found: C 65.45, H 7.00.

2.4 Phosphatases and phosphopeptides:

PTPRD, PTPRS and PTPRF phosphatase proteins (>95% purity) that are active in hydrolyzing pNPP substrate were produced in *E Coli* from His-tagged constructs and

purified as described [39,40]. We purchased PTPRJ and PTPN1 (PTP1B) (R&D Systems, Minneapolis MN).

2.5 Phosphatase assays:

Data for each assay type (3 wells/experimental condition, read using a Spectromax plate reader) was plotted vs time, and results derived from the slopes of linear regions were reported from triplicate independent experiments. pNPP dephosphorylation to pnitrophenolate was analyzed using pNPP substrate, 405 nm detection of the dephosphorylation product, controls with 5×10^{-5} M 7-BIA and 18 min incubations as described [22]. For assays of 7-BIA related ligands that were likely to inhibit in pseudoirreversible fashions, we also added 18 min preincubations.

2.6 Small molecule in silico docking:

The structure of the PTPRD phosphatase D1 (PDB ID 2NV5) was downloaded from the PDB database [41]. The model of the PTPRD phosphatase domain was prepared for docking by adding hydrogens, assigning protonation states and optimizing hydrogen bonds using the Schrodinger Protein Preparation Wizard [42,43]. 7-BIA analogs modeled as covalent binders were prepared in their final, covalently-bound states. All small molecules were prepared using LigPrep to enumerate protonation and tautomerization states and to generate initial 3D structures.

A model of illudalic acid covalently bound to the active site of PTPRD was generated based on [34]. The catalytic cysteine side chain was removed and illudalic acid docked using Glide [42,44,45], with a positional constraint of 3.2–4.7 Å from the alpha carbon of the catalytic cysteine allowing identification of poses that contain an atom within 1.5 Å of the position of the catalytic cysteine's sulfur. The cysteine side chain was modeled back in, a covalent bond was formed and the covalent-bound model was subjected to minimization using Prime [42,46,47]. After removal of the ligand and the catalytic cysteine, this model was used to generate a receptor to dock 7-BIA and its analogs. These compounds were docked using Glide with its extra precision (XP) protocol and a core constraint of the fused ring.

2.7 Activity at sites of action of other drugs.

Was tested in EUROFINs assays for sites of action (and side effects) of most marketed drugs [48]

2.8 Absorption studies:

To characterize the absorption of **58** *in vivo* we administered 10 mg/kg doses in 10 %DMSO/30% PEG-400 (Fluka)/60% aqueous solutions containing 40% β-cyclodextrin sulfobutyl ether sodium salts (Captisol, Selleckchem) intravenously, intraperitoneally or orally (gavage) to 7–9 week old male Sprague Dawley rats (Vital River, Zhejiang PRC). Rats were sacrificed using CO₂ after varying intervals and plasma was sampled *via* cardiac puncture. 50 μL of plasma were combined with 5 μL 50% methanol with 0.5% formic acid and 200 μL of acetonitrile containing LL-120001-NX or tolbutamide internal standards (*eg* compound **58**; 10 ng/mL) was added. Mixtures were vortexed for 1 min and centrifuged at 4000 rpm for 15 mins. 5 or 7.5 μL supernatant samples (plasma and brain, respectively)

were analyzed using an AB Sciex Triple Quad 5500 LC/MS/MS with Analyst 1.6.3 software, negative ion electrospray and multiple reaction monitoring scan mode with 293.10/192.00 for 7-BIA and 327.08/269.00 for the internal standard. Chromatography @ 0.4 mL/min used a Waters Acquity Ultra Performance LC System, Acquity UPLC BEH C18 column (1.7 μ m, 100 \times 2.1 mm), mobile phase A 1 mM NH₄OAc in water (declining from 90% to 5% and returning to 90% during 4–4.5 min room temperature runs) and mobile Phase B acetonitrile. Results were summed from peaks corresponding to open and closed forms of **58** and were compared to standard curves generated from plasma from untreated animals spiked with 5–10000 ng authentic **58**. The lower limit of quantitation was 5 ng/ml.

2.9 Tolerability studies:

To characterize dose related toxicities of **58**, we administered 200, 400, 600, 1000 and 2000 mg/kg oral doses to wildtype C57BL/6J (Jax) or PTPRD knockout mice backcrossed for >12 generations on this same C57BL/6J genetic background [21,49] of both genders which were bred and genotyped as described [22] *via* gavage in work approved by the New Mexico VA Healthcare System Institutional Animal Care and Use Committee. Mice and their spontaneous home cage behaviors were examined over the next three days (GRU, MM) then sacrificed by cervical dislocation and examined at necropsy. Major organs were fixed in 4% depolymerized paraformaldehyde, embedded in paraffin and sectioned. Slides from these tissue sections were examined by veterinary pathologists (New Mexico Department of Agriculture Veterinary Diagnostic Services Division [50]) after staining with hematoxylin and eosin and other stains.

3. Results

3.1. Structure-activity studies

Initial Deconstruction Efforts.—To improve our understanding of the interactions required for inhibiting PTPRD, we tested a number of the intermediates used in the original synthesis of 7-BIA (**2–4**) (Fig. 2) [22]. Unfortunately, none of these analogs were found to interact potently with PTPRD ($IC_{50} > 10 \mu$ M). Next, we evaluated a number of compounds that were expected to serve as potential covalent modifiers of PTPRD (**5–12**) but none of them showed desired potency. Previous work suggested that illudalic acid analogs employ pseudo irreversible mechanisms to inhibit PTPRD [22] in ways that are consistent with the postulated actions of 7-BIA on PTPRF's phosphatase [34]. The kinetics of PTPRF inhibition by illudalic acid were found to be consistent with a two-step mechanism in which the inhibitor and enzyme first interact noncovalently followed by covalent ligation [51]. However, neither these compounds, **13** or **14**, were active ($IC_{50} > 10 \mu$ M).

To test the importance of the lactol moiety present in 7-BIA (**1**), we evaluated benzopyran **15**. **15** was inactive at PTPRD ($IC_{50} > 10 \mu$ M). Having established the importance of the lactol moiety in 7-BIA, we removed the 5-carboxaldehyde, 6-methoxy and 7-butoxy groups (**21**). Each of these removals led to complete loss of activity at PTPRD ($IC_{50} > 10 \mu$ M). We also found that activity was lost if: (1) the 3-hydroxy from the 3-oxoisochromane nucleus was eliminated (**22**) or (2) the 6-methoxy group was homologated to a 6-ethoxy group

(**23**) or 6-butoxy group (**24**). These latter results confirmed the importance of 6-position substituents.

Having established the importance of the 3-, 5-, and 6-position groups, we focused on the role of the 7-butoxy group of 7-BIA. Removal of the 7-butoxy group (**25**) or its conversion to a methoxy group (**26**) were not well tolerated at PTPRD ($IC_{50} > 10 \mu M$). This suggested that the 7-butoxy group was critical for activity at PTPRD. To elucidate structural/activity relationships for this important 7-position, we conducted more detailed investigations of the influence of different 7-position substituents.

3.2 Investigation of 7-Position Substituent.

Analogs **27–61** were prepared from the commercially-available indanone **62** (Fig. 3). Treatment of indanone **62** with benzyl bromide under basic conditions followed by reduction with sodium borohydride to give the corresponding alcohol and dehydration in the presence of *p*-toluenesulfonic acid gave alkene **63**. Dihydroxylation of the olefin with AD-mix- α in the presence of methanesulfonamide followed by hydrogenolysis gave triol **64** [34]. Alkylation of **64** with the appropriate halide under basic conditions gave ethers of general structure **65**. Saponification of **65** followed by oxidation with sodium periodate ($NaIO_4$) gave lactols **27–51** and **53–61**. Treatment of triol **64** with phenyl triflimide ($PhNTf_2$) gave triflate **66** which was then treated with *trans*-1-penten-1-ylboronic acid pinacol ester in presence of palladium tetrakis to afford alkene **67**. Saponification, metal catalyzed hydrogenation, and oxidation with $NaIO_4$ provided pentyl analog **52**.

With our series of 7-position analogs in hand, we evaluated their ability to inhibit pNPP hydrolysis by PTPRD phosphatase (Table 1). To add opportunities for subsequent modifications, we extended the methoxy group to a benzyl group (**27**). Excitingly, **27** was found to have reasonable activity at PTPRD ($IC_{50} = 1.44 \mu M$).

Having identified an analog with promising activity, we examined a series of modifications to the benzene ring of **27** (Fig. 4). Addition of a 4-methyl group (**28**) decreased activity compared to **27** ($IC_{50} = 3.57 \mu M$ vs. $IC_{50} = 1.43 \mu M$). Conversion of the 4-methyl to 4-methoxy group (**29**) further decreased activity ($IC_{50} = 10–100 \mu M$). Movement of the position of the methoxy group (**30**, **31**) provided no improvement in PTPRD activity. Replacement of the 4-methyl group with nitrile (**32**), trifluoromethyl (**33**), trifluoromethoxy (**34**), fluoro (**35**), or iodo (**36**) substituents reduced activity ($IC_{50} > 10 \mu M$). However, activity was seen with conversion to the bromo (**37**) ($IC_{50} = 2.62 \mu M$), suggesting that additional lipophilicity might be favored. To this end, we explored the addition of multiple chlorine atoms to **27**. To our delight, the 2,4-dichloro analog **38** displayed increased activity relative to **27** ($IC_{50} = 0.97 \mu M$ vs. $IC_{50} = 1.43 \mu M$). The 3,4-dichloro analog **39** was less active than **38** ($IC_{50} > 10 \mu M$ vs. $IC_{50} = 0.97 \mu M$). See also Table 3.

Interestingly, we found that replacement of the 4-methyl with a 4-phenoxy group (**40**) increased PTPRD activity ($IC_{50} = 1.06 \mu M$ vs. $IC_{50} = 3.57 \mu M$). Addition of a 4'-fluoro group (**41**) decreased activity compared to **40** ($IC_{50} = 4.18 \mu M$ vs. $IC_{50} = 1.06 \mu M$). The latter finding was not unexpected given the loss of activity seen with **23**. However, this suggested that **40** was binding in a manner similar to **1**. Bioisosteric replacement of the

benzene ring in **28** with a thiophene (**42**) was tolerated ($IC_{50} = 4.05 \mu\text{M}$ vs. $IC_{50} = 3.57 \mu\text{M}$). However, replacement of the 2-methylthiophene ring in **42** with a 2-chlorothiazole ring (**43**) abolished activity ($IC_{50} > 50 \mu\text{M}$).

Conversion of the benzyl group in **27** to a 2-naphthyl group (**44**) was well tolerated at PTPRD ($IC_{50} = 2.05 \mu\text{M}$ vs. $IC_{50} = 1.44 \mu\text{M}$). Extension of the benzyl group to a phenethyl group (**45**) was examined. Although this modification was not well tolerated ($IC_{50} > 10 \mu\text{M}$), bioisosteric replacement of the phenyl ring with a 1-pyrrole (**46**) restored some activity ($IC_{50} = 3.20 \mu\text{M}$). Homologation of the ethyl linker to a propyl linker (**47**) further increased activity relative to **45** ($IC_{50} = 1.82 \mu\text{M}$ and $IC_{50} > 10 \mu\text{M}$).

We explored a series of modifications to the butoxy chain of 7-BIA (**1**). Addition of a 4-chlorophenyl group to the terminal carbon of **1** (**48**) was tolerated ($IC_{50} = 3.03 \mu\text{M}$ vs. $IC_{50} = 2.29 \mu\text{M}$). Conversion of the chloro group to the fluoro group (**49**) further increased PTPRD activity compared to **1** ($IC_{50} = 1.33 \mu\text{M}$ vs. $IC_{50} = 2.29 \mu\text{M}$). Addition of a methyl group to the 3-position of the butyl chain in **1** (**50**) was tolerated ($IC_{50} = 2.33 \mu\text{M}$ vs. $IC_{50} = 2.29 \mu\text{M}$). Introduction of an alkene to **50** (**51**) provided no enhancement of activity ($IC_{50} = 2.30 \mu\text{M}$ vs. $IC_{50} = 2.33 \mu\text{M}$). Replacement of the oxygen in the butoxy group with a carbon (**52**) or introduction of an additional oxygen atom to the butoxy chain (**53**) abolished PTPRD activity ($IC_{50} > 100 \mu\text{M}$). Addition of a fluorine atom to the terminal carbon of the butoxy chain in **1** (**54**) was well tolerated ($IC_{50} = 2.41 \mu\text{M}$ vs. $IC_{50} = 2.29 \mu\text{M}$). However, adding two additional fluorine atoms (**55**) decreased activity compared to **54** ($IC_{50} = 4.65 \mu\text{M}$ vs. $IC_{50} = 2.41 \mu\text{M}$).

The series of analogs (**56–61**) (Fig. 5) explored the role of conformation constraint in the 7-butoxy group in **1**. Replacement of butyl group with cyclopropylmethyl (**56**) abolished PTPRD activity ($IC_{50} > 100 \mu\text{M}$). However, the homologation of the cyclopropylmethyl group to a cyclobutylmethyl (**57**) restored PTPRD activity to a level comparable to **1** ($IC_{50} = 1.80 \mu\text{M}$ vs. $IC_{50} = 2.29 \mu\text{M}$). To our delight, homologation of the cyclobutylmethyl group to a cyclopentylmethyl group (**58**, termed NHB-1109) further enhanced PTPRD activity compared to **57** ($IC_{50} = 0.69 \mu\text{M}$ vs. $IC_{50} = 1.80 \mu\text{M}$) (Fig. 6). Extending the cyclopentane ring in **58** to a cyclohexane ring (**59**) or a cycloheptane ring (**60**) decreased activity ($IC_{50} = 0.86 \mu\text{M}$ and $IC_{50} = 1.47 \mu\text{M}$, respectively vs. $IC_{50} 0.69 \mu\text{M}$). Replacement of the pentane ring in **58** with a bicyclo[1.1.1] pentane (**61**) modestly reduced potency at PTPRD compared to **58** ($IC_{50} = 3.36 \mu\text{M}$ vs. $IC_{50} = 0.69 \mu\text{M}$). Interestingly, the phenyl ring mimic **61** was also found to have reduced activity vs. **27** ($IC_{50} = 3.36 \mu\text{M}$ vs. $IC_{50} = 1.64 \mu\text{M}$).

3.3 Relative activities at selected phosphatases.

We tested the specificities of the 7-position substituted analogs with $IC_{50} \sim 5 \mu\text{M}$, and of **1** itself, at several other protein tyrosine phosphatases (Table 2). There were modest differences in the relative potencies of many of these compounds at PTPRD, PTPRS and PTPRF, the three members of the “LAR” subfamily of receptor type protein tyrosine phosphatases. **1** and several other 7-position substituted compounds displayed moderate potencies at PTPRJ. While several analogs displayed activity at PTP1B (PTPN1), a major

target for diabetes medication development [52], other analogs lacked substantial potency at PTP1B.

Comparison of activities of the cyclopropyl-, cyclobutyl-, cyclopentyl-, cyclohexyl- and cycloheptyl- methoxy 7-position substitutions (**56–60**) appears especially informative. The five and six membered rings provided optimal potency at PTPRD's phosphatase while the lower cyclopentyl potency at PTPRJ and PTPN1/PTP1B made the cyclopentyl NHB1109 (**58**) the favored analog. The cyclopentyl NHB1109 (**58**) thus displayed greater selectivity for PTPRD vs PTPRS, PTPRF, PTPRJ and PTPN1/PTP1B than 7-BIA (1.6, 1.4, 3.5 and 1.8-fold, respectively).

3.4 *In silico* modeling.

We covalently docked interesting analogs to PTPRD's phosphatase *in silico*. While the core scaffold makes common van der Waals interactions as shown (Fig. 7), it also provides hydrogen bond interactions with glycine 1558, arginine 1559 and glutamine 1597. It has ionic interactions with arginine 1462, arginine 1559 and lysine 1464. These docking studies reveal differential interactions of 7-position substituents within two phosphatase sub-pockets. Smaller and/or more flexible 7-position substituents interact *in silico* with a sub-pocket at the foot of the phosphatase's WPD loop (Fig. 7, top). By contrast, docked models of the diphenyl ether (**40**) do not fit well in this pocket. Instead, the diphenyl ether moiety appears to interact with a different "antiWPD" pocket, located opposite the sub-pocket at the "foot of WPD loop" (Fig. 7, bottom). This anti-WPD binding is aided by pi-pi and hydrogen bond interactions with tyrosine 1386.

Many of the 7-position analogs that display potency at PTPRD appear to occupy the pocket located near the foot of the phosphatase's "WPD loop". They orient nitrogens from the key phosphatase arginine 1333 (R1333) toward the direction of this pocket. By contrast, diphenylether **40** and related compounds that occupy the "anti-WPD" pocket orient the R1333 nitrogen toward this the "anti-WPD" pocket. While these data suggest that 7-BIA related compounds with 7-position substitutions that optimally occupy the anti-WPD pocket may provide suitable PTPRD phosphatase inhibitors, the relatively high potency of **40** in inhibiting PTPN1/PTP1B causes cautions for this approach.

Although compounds with low Coulomb energies tended to be inactive, docking scores of these compounds fit only modestly with *in vitro* potencies. Correlations between these *in silico* values and potencies determined *in vitro* failed to reach significance ($\rho = 0.28$, one tailed $p = 0.38$). Given the strongly-electropositive binding pocket, it may not be surprising that Coulomb energy correlate best with activity. Likewise, the modest correlation between docking score and activity is not surprising given that structures were not preconfigured for ligand binding. Refined models in which a covalent bond is added and interfaces minimized can help to explain the structure activity relationships identified within series of compounds. For example, the changes in activity with respect to ring size suggest that the cyclopentyl substituent fits the WPD loop pocket well and allows this loop to close over it. By contrast, smaller rings underfill the pocket and larger rings overfill it,

Together, our data supports models whereby illudalic acid-related compounds are first recognized by the phosphatase and then rearrange to provide covalent interactions with the catalytic cysteine, resulting in pseudo irreversible inhibition of the phosphatase [34,35].

3.4 Activity at sites of action of other drugs.

We tested activities of NHB1109 (**58**) in EUROFINs assays for sites of action (and side effects) of most marketed drugs. There was no activity with EC_{50} 100 μ M at any of these sites.

3.5 Absorption and preliminary estimates of terminal plasma half-life:

Peaks that we interpreted as open and closed forms of **58** were detected in rat plasma following intravenous, intraperitoneal or oral (gavage) administration of 10 mg/kg doses. Plasma levels were 24633, 92.6 and 1.03 ng/g at 5, 30 and 240 min after intravenous administration. Levels were 577, 10.3 and 1.84 ng/g at 30, 120 and 240 min after intraperitoneal administration. They were 82.4, 24.2 and 4.62 ng/g at 30, 120 and 240 min after gavage. These values provided preliminary estimates of a terminal half-life of about 50 min for NHB1109 (**58**).

3.6 Identification of gross toxicity and no observed adverse effect level (NOAEL) in wildtype and PTPRD knockout mice:

We dosed wildtype C57BL/6J (Jax) or PTPRD knockout mice backcrossed for > 12 generations on this same C57BL/6J genetic background [21,49] of both genders by gavage, observed them (GRU and MM) over three days for survival (or inanition sufficient to require euthanasia), weight and obvious changes in behavior in their cages then sacrificed the remaining mice. Gross pathological examination by our veterinarian was followed by major organ histopathology performed by veterinary pathologists. Mice (n = 3–6) with doses to 200 mg/kg of both genders revealed no changes in home cage behaviors that were obvious to nonblinded observers familiar with the behaviors of these strains. There were no changes in gross examination. There was no organ toxicity on histopathological examination.

All mice which received 2000 or 1000 mg/kg gavage doses and 1/3 of mice dosed with 400 and 600 mg/kg doses lost weight, reduced their oral intake, developed abdominal distension that was visible on examination during life and revealed distended stomachs and small intestines on necropsies. None of these mice displayed major organ histopathological abnormalities, however. These changes resulted in death (or euthanasia) prior to day 3 of 60% of mice dosed with 2000 mg/kg NHB1109, 40% of the mice dosed with 1000 mg/kg, 33% of mice dosed with 600 mg/kg but none that received 400 or 200 mg/kg doses. Heterozygous and homozygous PTPRD knockout mice (n = 3–4 each) displayed this same constellation of findings that we term “ileus”. Mice treated with 2000 mg/kg lost 17 g prior to euthanasia (p = 0.001 vs vehicle treated mice which lost 1.7 g on average over three days). Losses vs vehicle treated mice did not reach significance for 1000 (9 g), 600 (1.1 g), 400 (3.4) or 200 (1.3 g) mg/kg NHB1109 doses. We thus set the mouse no observed adverse effect level (NOAEL) for single NHB1109 (**58**) doses at 200 mg/kg p.o. based on weight changes and these qualitative observations of gross pathology, histopathology and cage behaviors.

4. Discussion

The structure activity studies reported here provide substantial novel information about the ways in which modifications of our initial small molecule illudalic acid analog 7-BIA (**1**) change interactions with the phosphatase from receptor type protein tyrosine phosphatase PTPRD as well as other key receptor- and nonreceptor type protein tyrosine phosphatases. Our identification of greater potencies and specificities of the 7-cyclopentylmethoxy analog **58** NHB1109 led us to identify relatively favorable features of this compound's absorption, plasma half-life and specificity vs targets of other drugs that are licensed for use in humans. These features, in turn, allowed us to identify the high doses that provide toxicity *in vivo*, and thus to establish a no adverse effect level in mice based on qualitative observations. Each of these data provides encouragement for further *in vivo* testing of effects in animal models relevant to addiction and further development of **58** NHB1109 toward use in humans.

While we were unable to produce potent inhibitors when we changed many aspects of **1** 7-BIA, we were able to identify a robust structure activity relationship for 7-position substitutions that resulted in multiple compounds with greater potency than 7-BIA as inhibitors of PTPRD. There were marked differences in selectivity for key off target phosphatases, especially PTPN1/PTP1B, for a number of these compounds. Taken together, these data help to define interactions of PTPRD and related phosphatases with NHB1109 **58**, 7-BIA **1** and related compounds. These specificity experiments also extend available structure–activity relationship data for PTPRF, PTPRS, PTPRJ and PTPN1 (PTP1B). Taken together, these data document substantial specificities for these interactions and guide development of improved inhibitors for not only PTPRD but also for these other phosphatases.

The potency, selectivity, lack of *in vivo* toxicity at doses to 200 mg/kg and reasonable biodistribution data for NHB1109 **58** supports interest in developing this compound further as a potential human antiaddiction therapeutic. Its combination of modest plasma half-life and likely pseudoirreversible mechanism of action should be advantageous for reducing the duration of systemic exposure while providing the prolonged physiological half-life that has aided, for example, success of depot opiate antagonist formulations [53].

The complex etiologies of substance use disorders include many features that can be only distantly related to the rewarding properties of addictive substances [54]. Rewarding properties of novel substances play substantial roles in placement of such substances on Drug Enforcement Agency schedules that mandate more or less constraints for prescribing in the United States [55]. However, no antiaddiction therapeutic has yet been licensed based solely on its ability to reduce reward from illicit or prescribed substances of abuse. As we and others develop small molecules that reduce reward from abused substances in animal models and (hopefully) identify such reductions in humans, we will need to consider appropriate pathways toward licensing of reward-reducing agents for prevention and treatment of substance use disorders. Ancillary Information

Acknowledgement

PTPRD knockout mice were generously provided by N Uetani and Y Iwakura. We received valuable advice and assistance from F I Carroll, A Sulima, K Rice, J Adair and O Kovbasnjuk. We are grateful to support from NIDA and NIA U01DA047713 and supplement, (J Acri and R Klein, program officers), the Biomedical Research Institute of New Mexico, the University of Maryland School of Medicine, the Baltimore Biomedical Research and Education Foundation and the New Mexico and Maryland VA Healthcare Systems.

Abbreviations:

pNPP	para nitrophenol phosphate
PTPRD	receptor type protein tyrosine phosphatase D
pY	phosphotyrosine
SNP	single nucleotide polymorphism

References

- [1]. Report of the President's Commission on Combatting Drug Addiction and the Opioid Crisis, 2017. https://trumpwhitehouse.archives.gov/sites/whitehouse.gov/files/images/final_report_draft_11-15-17.pdf.
- [2]. <https://www.psychcongress.com/article/hhs-official-fourth-wave-looms-drug-crisis>.
- [3]. Fahs S, Lujan P, Köhn M, Approaches to Study Phosphatases, ACS Chem. Biol 11 (11) (2016) 2944–2961. [PubMed: 27700050]
- [4]. Yu Z-H, Zhang Z-Y, Regulatory Mechanisms and Novel Therapeutic Targeting Strategies for Protein Tyrosine Phosphatases, Chem. Rev 118 (3) (2018) 1069–1091. [PubMed: 28541680]
- [5]. Köhn M, Turn and Face the Strange: A New View on Phosphatases, ACS Cent. Sci 6 (4) (2020) 467–477. [PubMed: 32341996]
- [6]. Mullard A, Phosphatases start shedding their stigma of undruggability, Nat. Rev. Drug Discovery 17 (12) (2018) 847–849. [PubMed: 30482950]
- [7]. Uhl GR, Martinez MJ, PTPRD: neurobiology, genetics, and initial pharmacology of a pleiotropic contributor to brain phenotypes, Ann. N Y Acad. Sci 1451 (1) (2019) 112–129. [PubMed: 30648269]
- [8]. Uhl GR, Drgonova J, Cell adhesion molecules: druggable targets for modulating the connectome and brain disorders? Neuropsychopharmacology 39 (1) (2014) 235.
- [9]. Liu Q-R, Drgon T, Walther D, Johnson C, Poleskaya O, Hess J, Uhl GR, Pooled association genome scanning: validation and use to identify addiction vulnerability loci in two samples, Proc. Natl. Acad. Sci. U S A 102 (33) (2005) 11864–11869. [PubMed: 16091475]
- [10]. Liu QR, Drgon T, Johnson C, Walther D, Hess J, Uhl GR, Addiction molecular genetics: 639,401 SNP whole genome association identifies many “cell adhesion” genes, Am. J. Med. Genet. B Neuropsychiatr. Genet 141B (8) (2006) 918–925. [PubMed: 17099884]
- [11]. Drgon T, Johnson CA, Nino M, Drgonova J, Walther DM, Uhl GR, “Replicated” genome wide association for dependence on illegal substances: genomic regions identified by overlapping clusters of nominally positive SNPs, Am. J. Med. Genet. B Neuropsychiatr. Genet 156 (2) (2011) 125–138. [PubMed: 21302341]
- [12]. Li D, Zhao H, Kranzler HR, Li MD, Jensen KP, Zayats T, Farrer LA, Gelernter J, Genome-wide association study of copy number variations (CNVs) with opioid dependence, Neuropsychopharmacology 40 (4) (2015) 1016–1026. [PubMed: 25345593]
- [13]. Jung JZH, Grant BF, Chou P, Identification of novel genetic variants of DMS5 alcohol use disorder: Genome wide association study in National Epidemiological Survey on Alcohol Related Conditions-III, Abstracts, World Congress of Psychiatry Genetics 2017.

- [14]. Uhl GR, Liu QR, Drgon T, Johnson C, Walther D, Rose JE, Molecular genetics of nicotine dependence and abstinence: whole genome association using 520,000 SNPs, *BMC Genet.* 8 (2007) 10. [PubMed: 17407593]
- [15]. Uhl GR, Liu QR, Drgon T, Johnson C, Walther D, Rose JE, David SP, Niaura R, Lerman C, Molecular genetics of successful smoking cessation: convergent genome-wide association study results, *Arch. Gen. Psychiatry* 65 (6) (2008) 683–693. [PubMed: 18519826]
- [16]. Cox JW, Sherva RM, Lunetta KL, Johnson EC, Martin NG, Degenhardt L, Agrawal A, Nelson EC, Kranzler HR, Gelernter J, Farrer LA, Genome-Wide Association Study of Opioid Cessation, *J. Clin. Med* 9 (1) (2020) 180, 10.3390/jcm9010180.
- [17]. Biernacka JM, Coombes BJ, Batzler A, Ho AM, Geske JR, Frank J, Hodgkinson C, Skime M, Colby C, Zillich L, Pozsonyiova S, Ho MF, Kiefer F, Rietschel M, Weinshilboum R, O'Malley SS, Mann K, Anton R, Goldman D, Karpyak VM, Genetic contributions to alcohol use disorder treatment outcomes: a genome-wide pharmacogenomics study, *Neuropsychopharmacology* (2021).
- [18]. Hart AB, Engelhardt BE, Wardle MC, Sokoloff G, Stephens M, de Wit H, Palmer AA, Genome-wide association study of d-amphetamine response in healthy volunteers identifies putative associations, including cadherin 13 (CDH13), *PLoS One* 7 (8) (2012).
- [19]. Hart A and Palmer A, personal communication, 2013.
- [20]. Joslyn G, Ravindranathan A, Brush G, Schuckit M, White RL, Human variation in alcohol response is influenced by variation in neuronal signaling genes, *Alcohol. Clin. Exp. Res* 34 (5) (2010) 800–812. [PubMed: 20201926]
- [21]. Drgonova J, Walther D, Wang KJ, Hartstein GL, Lochte B, Troncoso J, Uetani N, Iwakura Y, Uhl GR, Mouse model for PTPRD associations with WED/RLS and addiction: reduced expression alters locomotion, sleep behaviors and cocaine-conditioned place preference, *Mol. Med* (2015).
- [22]. Uhl GR, Martinez MJ, Paik P, Sulima A, Bi G-H, Iyer MR, Gardner E, Rice KC, Xi Z-X, Cocaine reward is reduced by decreased expression of receptor-type protein tyrosine phosphatase D (PTPRD) and by a novel PTPRD antagonist, *Proc. Natl. Acad. Sci. U S A* 115 (45) (2018) 11597–11602. [PubMed: 30348770]
- [23]. Levin E and GRU, in preparation.
- [24]. Um JW, Ko J, LAR-RPTPs: synaptic adhesion molecules that shape synapse development, *Trends Cell Biol.* 23 (10) (2013) 465–475. [PubMed: 23916315]
- [25]. Takahashi H, Craig AM, Protein tyrosine phosphatases PTPdelta, PTPsigma, and LAR: presynaptic hubs for synapse organization, *Trends Neurosci.* 36 (9) (2013) 522–534. [PubMed: 23835198]
- [26]. Yamagata A, Sato Y, Goto-Ito S, Uemura T, Maeda A, Shiroshima T, Yoshida T, Fukai S, Structure of Slitrk2-PTPdelta complex reveals mechanisms for splicing-dependent trans-synaptic adhesion, *Sci. Rep* 5 (2015) 9686. [PubMed: 25989451]
- [27]. Yoshida T, Shiroshima T, Lee S-J, Yasumura M, Uemura T, Chen X, Iwakura Y, Mishina M, Interleukin-1 receptor accessory protein organizes neuronal synaptogenesis as a cell adhesion molecule, *J. Neurosci* 32 (8) (2012) 2588–2600. [PubMed: 22357843]
- [28]. Kwon SK, Woo J, Kim SY, Kim H, Kim E, Trans-synaptic adhesions between netrin-G ligand-3 (NGL-3) and receptor tyrosine phosphatases LAR, protein-tyrosine phosphatase delta (PTPdelta), and PTPsigma via specific domains regulate excitatory synapse formation, *J. Biol. Chem* 285 (18) (2010) 13966–13978. [PubMed: 20139422]
- [29]. Lin Z, Liu J, Ding H, Xu F, Liu H, Structural basis of SALM5-induced PTPdelta dimerization for synaptic differentiation, *Nat. Commun* 9 (1) (2018) 268. [PubMed: 29348579]
- [30]. Choi Y, Nam J, Whitcomb DJ, Song YS, Kim D, Jeon S, Um JW, Lee SG, Woo J, Kwon SK, Li Y, Mah W, Kim HM, Ko J, Cho K, Kim E, SALM5 trans-synaptically interacts with LAR-RPTPs in a splicing-dependent manner to regulate synapse development, *Sci. Rep* 6 (2016) 26676. [PubMed: 27225731]
- [31]. <https://biorxiv.org/cgi/content/short/2021.03.02.433536v1>.
- [32]. Wang J, Bixby JL, Receptor tyrosine phosphatase-delta is a homophilic, neurite-promoting cell adhesion molecular for CNS neurons, *Mol. Cell. Neurosci* 14 (4–5) (1999) 370–384. [PubMed: 10588391]

- [33]. Allen brain atlas images.
- [34]. Ling Q, Huang Y, Zhou Y, Cai Z, Xiong B, Zhang Y, Ma L, Wang X, Li X, Li J, Shen J, Illudalic acid as a potential LAR inhibitor: synthesis, SAR, and preliminary studies on the mechanism of action, *Bioorg. Med. Chem* 16 (15) (2008) 7399–7409. [PubMed: 18579388]
- [35]. Ling Q, Zhou YY, Cai ZL, Zhang YH, Xiong B, Ma LP, Wang X, Li X, Li J, Shen JK, Synthesis and LAR inhibition of 7-alkoxy analogues of illudalic acid, *Yao Xue Xue Bao* 45 (11) (2010) 1385–1397. [PubMed: 21355526]
- [36]. Nair MSR, Takeshita H, McMorris TC, Anchel M, Metabolites of *Clitocybe illudens*. IV. Illudalic acid, a sesquiterpenoid, and illudinine, a sesquiterpenoid alkaloid, *J. Organic Chem* 34 (1) (1969) 240–243.
- [37]. Woodward RB, Hoyer TR, Total synthesis of illudinine, illudalic acid, and illudacetic acid, *J. Am. Chem. Soc* 99 (24) (1977) 8007–8014.
- [38]. <https://www.eurofindiscoveryservices.com/services/in-vitro-assays>.
- [39]. Sequences available from the authors on request.
- [40]. Biomatic, sequences available from the authors on request.
- [41]. Almo SC, Bonanno JB, Sauder JM, Emtage S, Dilorenzo TP, Malashkevich V, Wasserman SR, Swaminathan S, Eswaramoorthy S, Agarwal R, Kumaran D, Madegowda M, Ragumani S, Patskovsky Y, Alvarado J, Ramagopal UA, Faber-Barata J, Chance MR, Sali A, Fiser A, Zhang Z.-yin., Lawrence DS, Burley SK, Structural genomics of protein phosphatases, *J. Struct. Funct. Genomics* 8 (2-3) (2007) 121–140. [PubMed: 18058037]
- [42]. Schrödinger Release 2019-4: Protein Preparation Wizard; Epik; Impact; Prime; Glide; LigPrep; Induced Fit Docking protocol, New York, NY, Schrödinger LLC, 2019.
- [43]. Madhavi Sastry G, Adzhigirey M, Day T, Annabhimoju R, Sherman W, Protein and ligand preparation: parameters, protocols, and influence on virtual screening enrichments, *J. Comput. Aided Mol. Des* 27 (3) (2013) 221–234. [PubMed: 23579614]
- [44]. Friesner RA, Murphy RB, Repasky MP, Frye LL, Greenwood JR, Halgren TA, Sanschagrin PC, Mainz DT, Extra precision glide: docking and scoring incorporating a model of hydrophobic enclosure for protein-ligand complexes, *J. Med. Chem* 49 (21) (2006) 6177–6196. [PubMed: 17034125]
- [45]. Halgren TA, Murphy RB, Friesner RA, Beard HS, Frye LL, Pollard WT, Banks JL, Glide: a new approach for rapid, accurate docking and scoring. 2. Enrichment factors in database screening, *J. Med. Chem* 47 (7) (2004) 1750–1759. [PubMed: 15027866]
- [46]. Jacobson MP, Friesner RA, Xiang Z, Honig B, On the role of the crystal environment in determining protein side-chain conformations, *J. Mol. Biol* 320 (3) (2002) 597–608. [PubMed: 12096912]
- [47]. Jacobson MP, Pincus DL, Rapp CS, Day TJF, Honig B, Shaw DE, Friesner RA, A hierarchical approach to all-atom protein loop prediction, *Proteins* 55 (2) (2004) 351–367. [PubMed: 15048827]
- [48]. <https://http://www.eurofindiscoveryservices.com/seerices/in-vitro-assays>.
- [49]. Uetani N, Kato K, Ogura H, Mizuno K, Kawano K, Mikoshiba K, Yakura H, Asano M, Iwakura Y, Impaired learning with enhanced hippocampal long-term potentiation in PTPdelta-deficient mice, *EMBO J.* 19 (12) (2000) 2775–2785. [PubMed: 10856223]
- [50]. <https://www.nmda.edu/nmda-homepage/divisions/vds/>.
- [51]. McCullough BS, Batsomboon P, Hutchinson KB, Dudley GB, Barrios AM, Synthesis and PTP Inhibitory Activity of Illudalic Acid and Its Methyl Ether, with Insights into Selectivity for LAR PTP over Other Tyrosine Phosphatases under Physiologically Relevant Conditions, *J. Nat. Prod* 82 (12) (2019) 3386–3393. [PubMed: 31809044]
- [52]. Thareja S, Aggarwal S, Bhardwaj TR, Kumar M, Protein tyrosine phosphatase 1B inhibitors: a molecular level legitimate approach for the management of diabetes mellitus, *Med. Res. Rev* 32 (3) (2012) 459–517. [PubMed: 20814956]
- [53]. Krupitsky E, Nunes EV, Ling W, Illeperuma A, Gastfriend DR, Silverman BL, Injectable extended-release naltrexone for opioid dependence: a double-blind, placebo-controlled, multicentre randomised trial, *Lancet* 377 (9776) (2011) 1506–1513. [PubMed: 21529928]

- [54]. Volkow ND, Michaelides M, Baler R, The Neuroscience of Drug Reward and Addiction, *Physiol. Rev* 99 (4) (2019) 2115–2140. [PubMed: 31507244]
- [55]. <https://www.dea.gov/drug-information/drug-scheduling>.

Author Manuscript

Author Manuscript

Author Manuscript

Author Manuscript

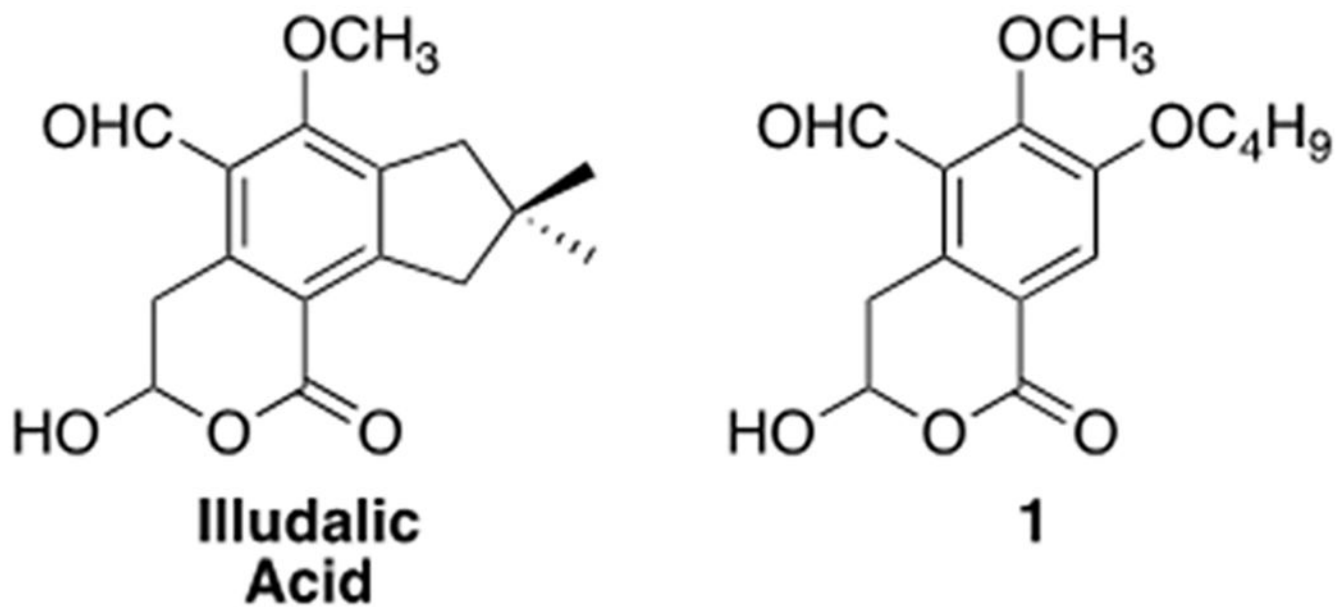


Fig. 1.
Structures of illudalic acid and 7-BIA (1).

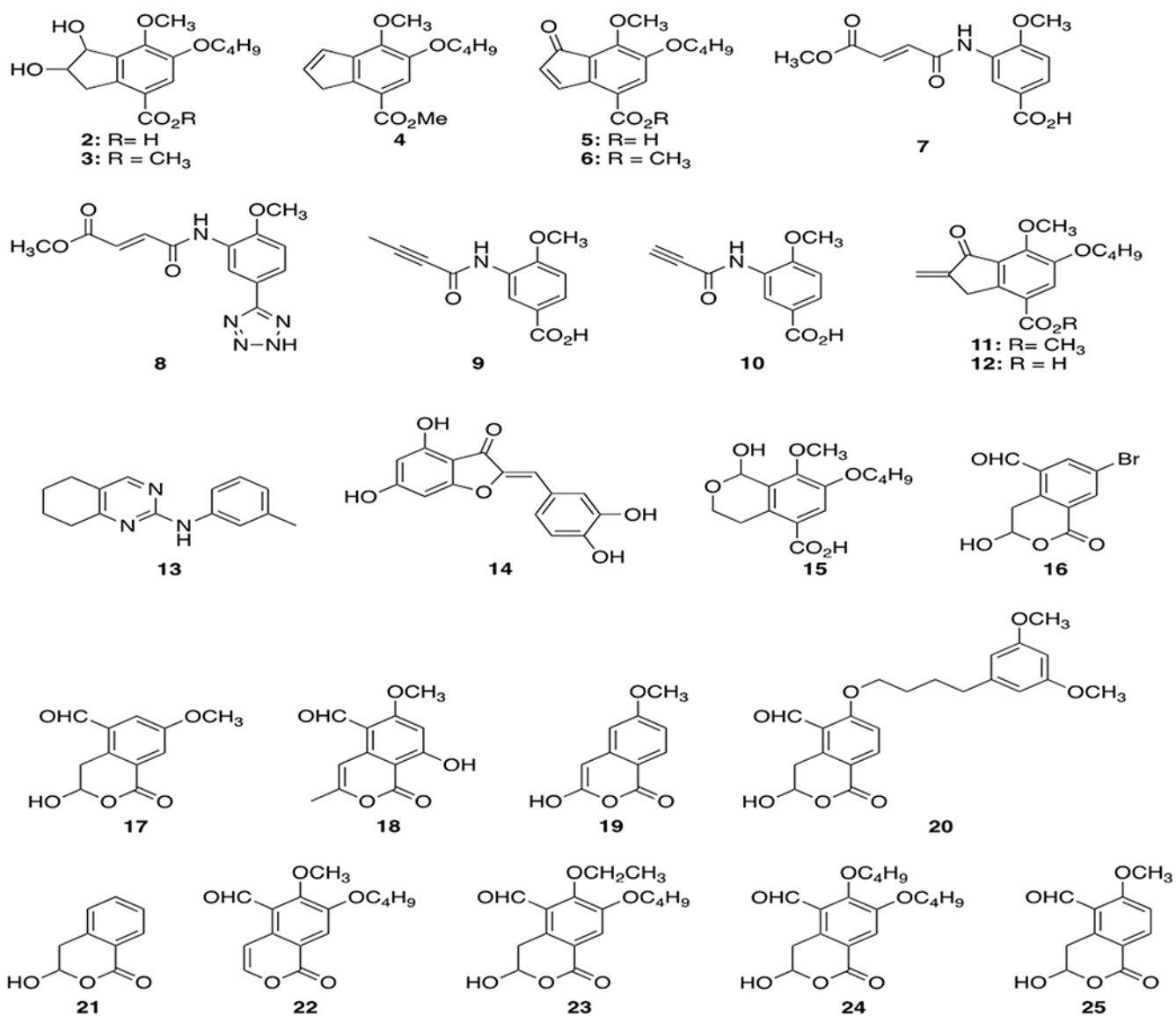


Fig. 2. Structures of compounds 2–25. Each of these compounds displayed $IC_{50} > 10 \mu M$ for inhibition of pNPP hydrolysis by recombinant human PTPRD phosphatase.

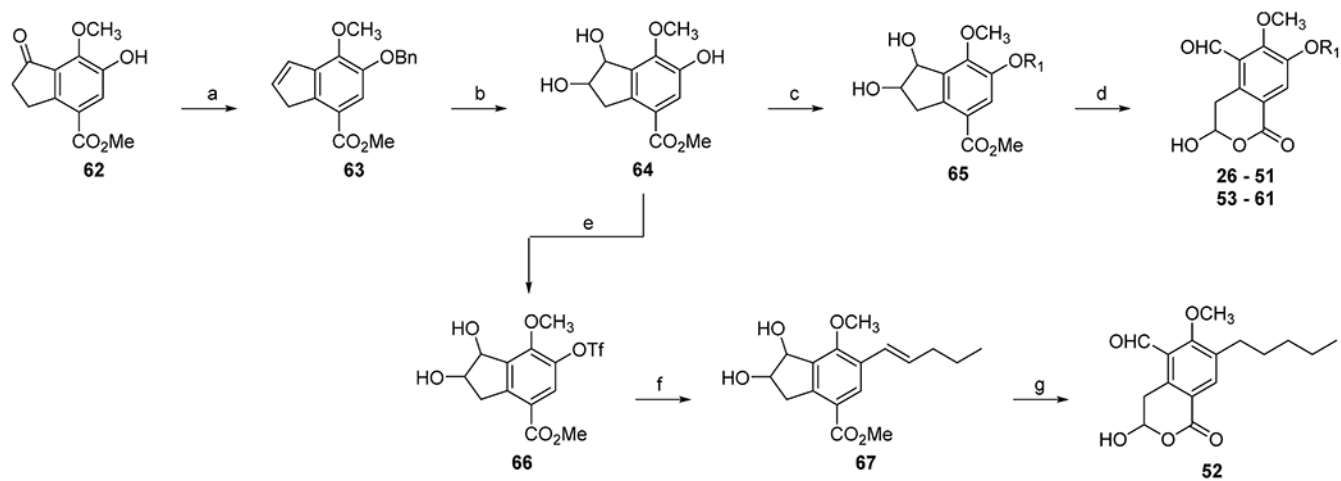
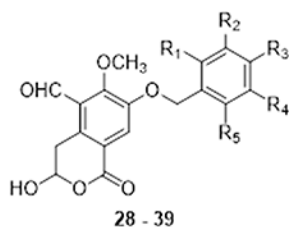
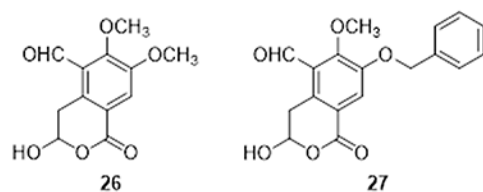


Fig. 3.
Synthesis of analogs 27–61.



28: R₁ = H; R₂ = H; R₃ = CH₃; R₄ = H; R₅ = H

29: R₁ = H; R₂ = H; R₃ = OCH₃; R₄ = H; R₅ = H

30: R₁ = H; R₂ = OCH₃; R₃ = H; R₄ = H; R₅ = H

31: R₁ = OCH₃; R₂ = H; R₃ = H; R₄ = H; R₅ = H

32: R₁ = H; R₂ = H; R₃ = CN; R₄ = H; R₅ = H

33: R₁ = H; R₂ = H; R₃ = CF₃; R₄ = H; R₅ = H

34: R₁ = H; R₂ = H; R₃ = OCF₃; R₄ = H; R₅ = H

35: R₁ = H; R₂ = H; R₃ = F; R₄ = H; R₅ = H

36: R₁ = H; R₂ = H; R₃ = I; R₄ = H; R₅ = H

37: R₁ = H; R₂ = H; R₃ = Br; R₄ = H; R₅ = H

38: R₁ = Cl; R₂ = H; R₃ = Cl; R₄ = H; R₅ = H

39: R₁ = H; R₂ = Cl; R₃ = Cl; R₄ = H; R₅ = H

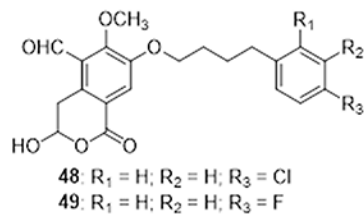
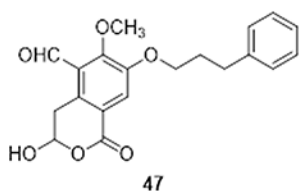
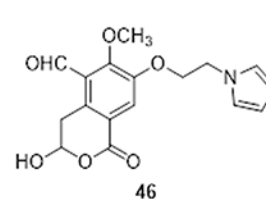
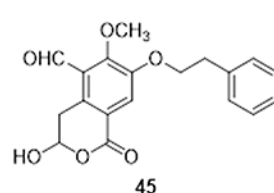
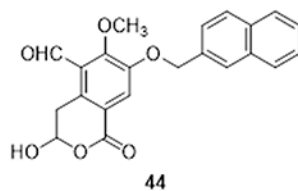
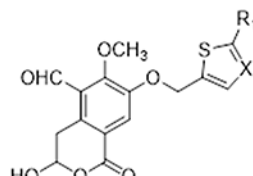
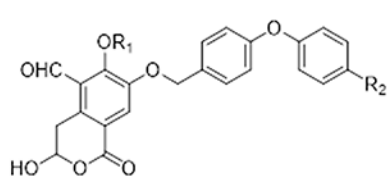


Fig. 4.
Structures of compounds 26–49.

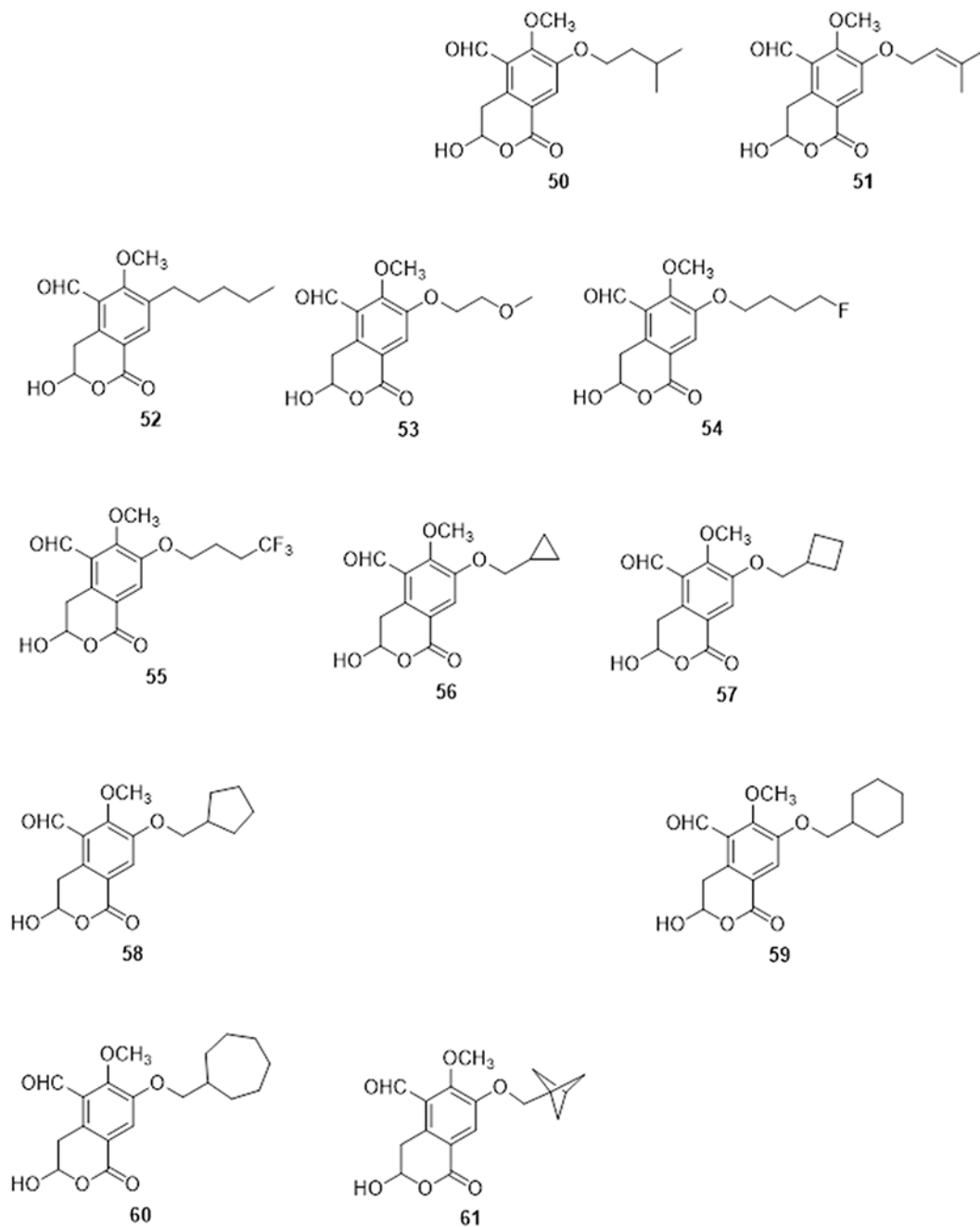


Fig. 5.
Structures of compounds **50–61**.

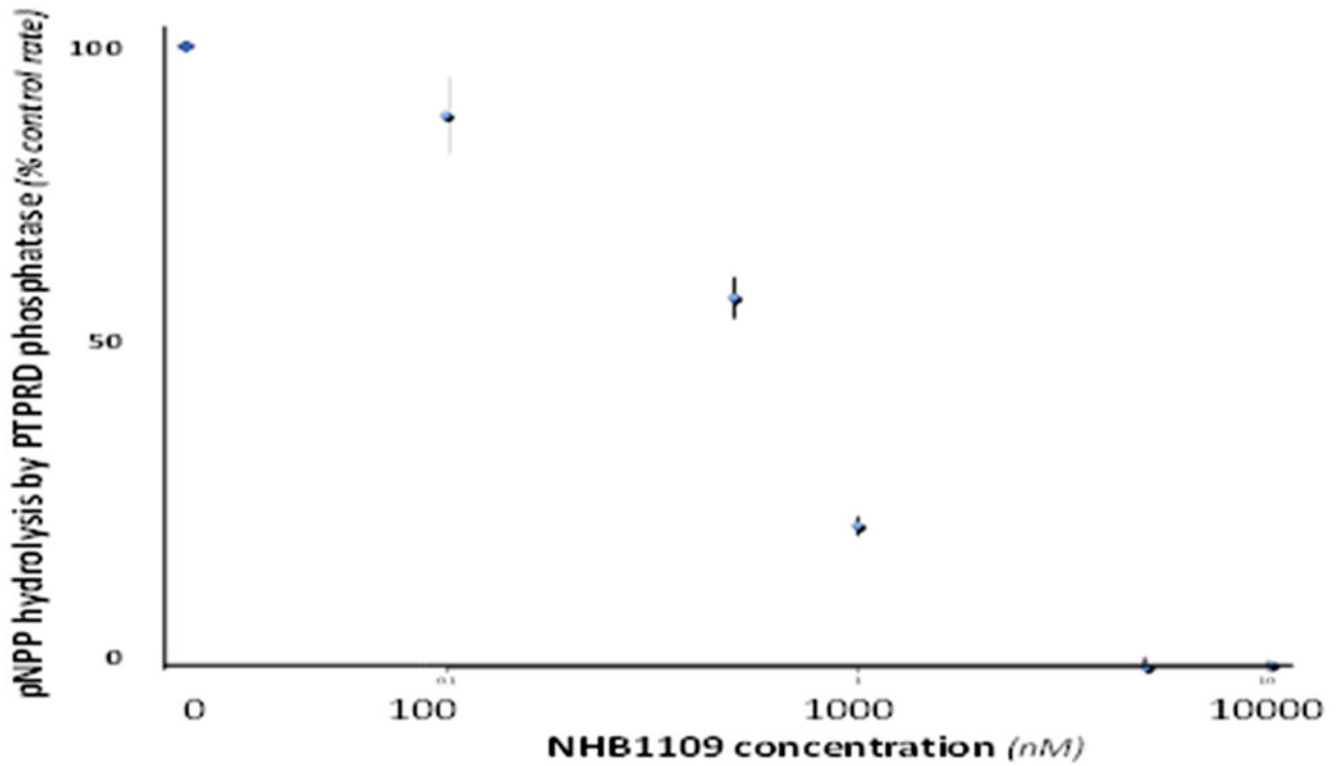


Fig. 6. Concentration/response data for NHB1109 inhibition of activity of recombinant human PTPRD phosphatase. % control rate of hydrolysis of pNPP substrate vs NHB1109 concentration (nM; mean \pm SEM) is shown.

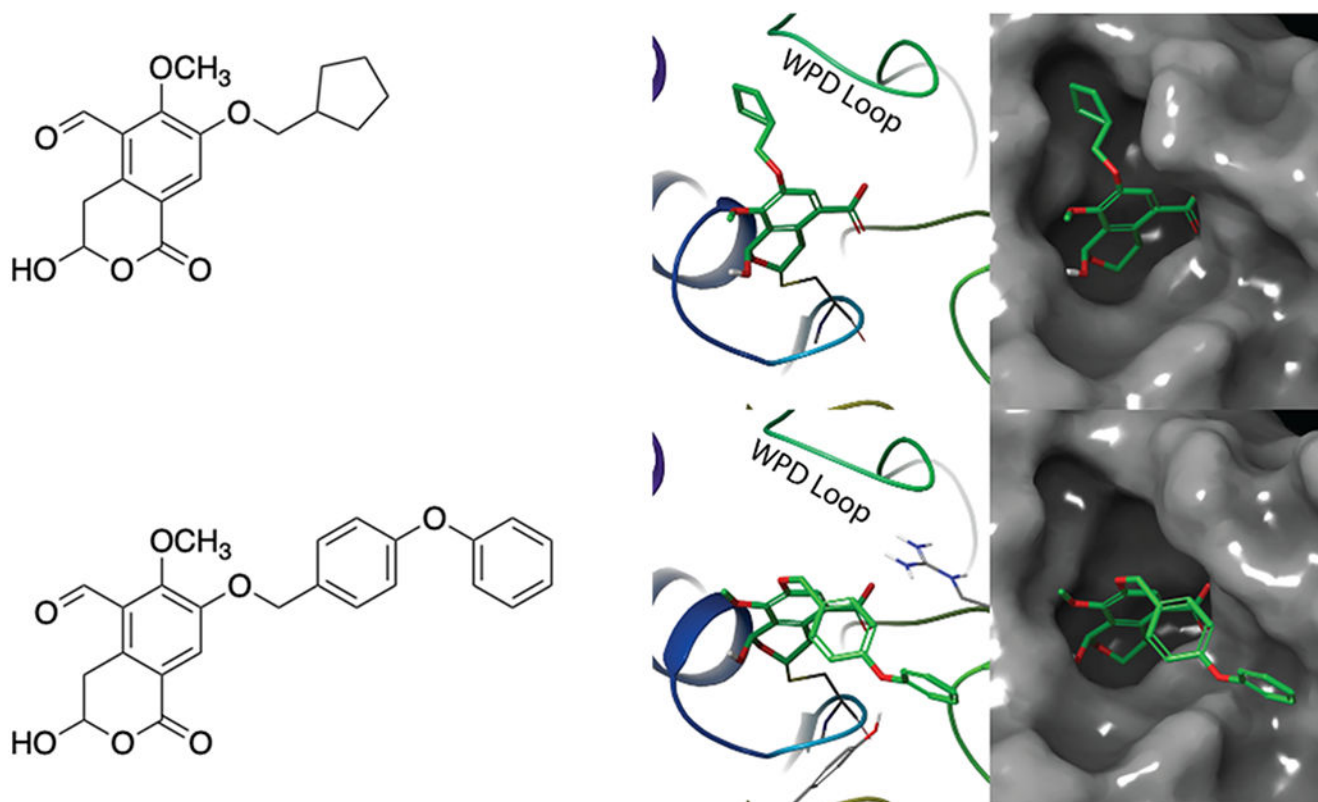
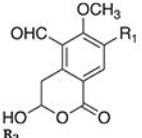
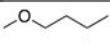
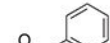
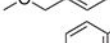
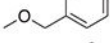
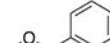
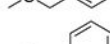
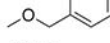
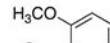
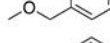
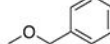

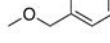

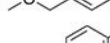
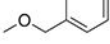

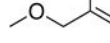


Fig. 7. *In silico* modeling for interactions of different 7-position substituents with a PTPRD phosphatase pocket at the foot of the WPD loop (modeled with a cyclopentylmethyl substituent compd **58**) vs the “anti-WPD” pocket (modeled with the diphenyl ether substituent compd **40**) Hydrogen bond interactions are represented as yellow dashes, aromatic hydrogen bonds are represented as purple dashes, salt bridge interactions are represented as blue dashes, and pi-pi interactions are represented as cyan dashes. (For interpretation of the references to colour in this figure legend, the reader is referred to the web version of this article.)

Table 1

IC₅₀ values of selected 7-position substituted 7-BIA analogs in inhibiting pNPP hydrolysis by recombinant PTPRD inhibiting PTPRD phosphatase in initial screening assays.

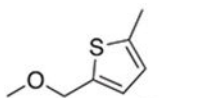
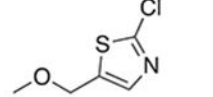
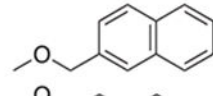
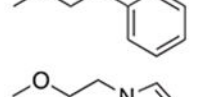

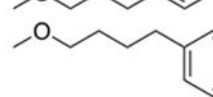
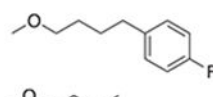
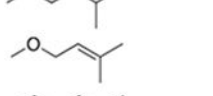
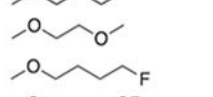
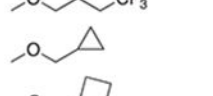
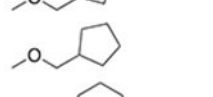





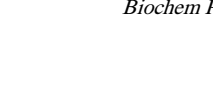

Cmpd		AVG PTPRD
1		2.295 (3.055, 1.495, 2.295)
27		1.435
28		3.575
29		10-100
30		4.120
31		> 100
32		>10
33		10.00
34		>50
35		>500
36		100-500
37		2.620
38		0.973
39		>10
40		1.063
41		4.180
42		4.047

Author Manuscript

Author Manuscript

Author Manuscript

Author Manuscript

43		>50
44		2.054
45		10.00
46		3.200
47		1.820
48		3.035
49		1.330
50		2.330
51		2.305
52		>100
53		31.350
54		2.410
55		4.650
56		>100
57		1.800
58		0.689
59		0.86
60		1.47
61		3.36

Author Manuscript

Author Manuscript

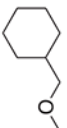
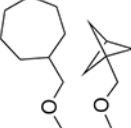
Author Manuscript

Author Manuscript

Table 2

IC₅₀ values (mean +/- SEM of three independent experiments) of 7-position substituted 7-BIA (1) analogs with IC₅₀ values < 10uM in inhibiting pNPP hydrolysis by recombinant PTPRD, PTPRF, PTPRS, PTPRJ and PTPN1 (PTP1B) phosphatases.

Compd		PTPRD	PTPRF	PTPRS	PTPRJ	PTP1B
1		2.27 (0.2)	3.95 (0.7)	1.27 (1)	27.4 (12.6)	215 (38.6)
27		1.64 (0.4)	3.62 (1.5)	1.60 (0.4)	47.17 (8.3)	
28		3.80 (1.3)	6.57 (0.3)	3.58 (1.2)	37.7 (11.6)	148.4 (39.4)
30		4.12		13.01		
37		2.62*	3.82*	5.00*	29.90*	
38		0.98 (0.0)	3.55 (1.2)	1.03 (0.2)	14.61	75.96 (5.2)
40		1.60 (0.29)	3.93(1.7)	1.34(0.34)	28.40	16.71 (7.11)
41		2.49*				
42		0.92*	3.50*	1.40*	19.83*	
44		2.05 (1)	5.87 (1.8)	4.61 (0.8)	33.29 (7.6)	221.3 (38.4)
45		4.57 (1.4)	4.24 (1)	3.03 (1.2)	54.85 (8.7)	4.57 (1.4)
46		3.20*				
47		1.82*	4.41*	0.93*		
48		2.22 (1.02)	5.67(1.3)	3.09(0.54)	28.94 (2.8)	65.74 (16.6)
50		2.82 (0.4)	3.87 (0.5)	2.76 (0.5)	51.91 (9.3)	120.67(27.6)
51		3.21 (1.1)	2.46 (0.1)	1.80 (0.7)	17.83 (9)	>100
55		4.65*				
56		4.18*				
57		1.80	3.03	3.36		5.82
58		0.69 (0.1)	1.72 (0.6)	0.61 (0.1)	29.3 (4.8)	119.2 (53)
59		0.86 (0.2)	0.76 (0.0)	1.06 (0.1)	0.56 (0.5)	100.5 (9.1)

60		1.47 (0.2)	0.77 (0.2)	1.16 (0.2)	9.81 (0.3)	27.1 (7.3)
61		3.36 (1.1)	2.09 (0.4)	3.55 (0.3)	21.03 (1.8)	214.97 (38.6)

* denotes compounds whose instability failed to allow valid triplicate experiments.

Values are mean \pm SEM of results from three independent experiments (each with triplicate samples) for compounds with PTPRD phosphatase IC₅₀ values < 5 μ M.

Table 3

Molecular formula strings for compounds described.

Compound	Smiles
1	<chem>OC(O)CC2=C(C=O)C(OC)=C(OCCCC)C=C2C1=O</chem>
2	<chem>OC(C(O)C1)C2=C1C(C(O)=O)=CC(OCCCC)=C2OC</chem>
3	<chem>OC(C(O)C1)C2=C1C(C(OC)=O)=CC(OCCCC)=C2OC</chem>
4	<chem>COC1=C(OCCCC)C=C(C(OC)=O)C2=C1C=CC2</chem>
5	<chem>O=C(C=C1)C2=C1C(C(O)=O)=CC(OCCCC)=C2OC</chem>
6	<chem>O=C(C=C1)C2=C1C(C(OC)=O)=CC(OCCCC)=C2OC</chem>
7	<chem>O=C(/C=C/C(OC)=O)NC1=CC(C(O)=O)=CC=C1OC</chem>
8	<chem>O=C(/C=C/C(OC)=O)NC1=CC(C2=NNN=N2)=CC=C1OC</chem>
9	<chem>O=C(C#CC)NC1=CC(C(O)=O)=CC=C1OC</chem>
10	<chem>O=C(C#C)NC1=CC(C(O)=O)=CC=C1OC</chem>
11	<chem>O=C(C(C1)=C)C2=C1C(C(OC)=O)=CC(OCCCC)=C2OC</chem>
12	<chem>O=C(C(C1)=C)C2=C1C(C(O)=O)=CC(OCCCC)=C2OC</chem>
13	<chem>CC1=CC=CC(NC2=NC3=C(CCCC3)C=N2)=C1</chem>
14	<chem>O=C(C1=C(O)C=C(O)C=C1O/2)C2=C\C3=CC=C(O)C(O)=C3</chem>
15	<chem>OC(OCC1)C2=C1C(C(O)=O)=CC(OCCCC)=C2OC</chem>
16	<chem>OC(O)CC2=C(C=O)C=C(Br)C=C2C1=O</chem>
17	<chem>OC(O)CC2=C(C=O)C=C(OC)C=C2C1=O</chem>
18	<chem>CC(O1)=CC2=C(C=O)C(OC)=CC(O)=C2C1=O</chem>
19	<chem>OC(O1)=CC2=CC(OC)=CC=C2C1=O</chem>
20	<chem>OC(O)CC2=C(C=O)C(OCCCC3=CC(OC)=CC(OC)=C3)=CC=C2C1=O</chem>
21	<chem>OC(O)CC2=CC=CC=C2C1=O</chem>
22	<chem>O=C1OC=CC2=C(C=O)C(OC)=C(OCCCC)C=C21</chem>
23	<chem>OC(O)CC2=C(C=O)C(OC)=C(OCCCC)C=C2C1=O</chem>
24	<chem>OC(O)CC2=C(C=O)C(OCCCC)=C(OCCCC)C=C2C1=O</chem>
25	<chem>OC(O)CC2=C(C=O)C(OC)=CC=C2C1=O</chem>
26	<chem>OC(O)CC2=C(C=O)C(OC)=C(OC)C=C2C1=O</chem>
27	<chem>OC(O)CC2=C(C=O)C(OC)=C(OCC3=CC=CC=C3)C=C2C1=O</chem>
28	<chem>OC(O)CC2=C(C=O)C(OC)=C(OCC3=CC=C(C)C=C3)C=C2C1=O</chem>
29	<chem>OC(O)CC2=C(C=O)C(OC)=C(OCC3=CC=C(OC)C=C3)C=C2C1=O</chem>
30	<chem>OC(O)CC2=C(C=O)C(OC)=C(OCC3=CC=CC(OC)=C3)C=C2C1=O</chem>
31	<chem>OC(O)CC2=C(C=O)C(OC)=C(OCC3=C(OC)C=CC=C3)C=C2C1=O</chem>
32	<chem>OC(O)CC2=C(C=O)C(OC)=C(OCC3=CC=C(C#N)C=C3)C=C2C1=O</chem>
33	<chem>OC(O)CC2=C(C=O)C(OC)=C(OCC3=CC=C(C(F)(F)F)C=C3)C=C2C1=O</chem>
34	<chem>OC(O)CC2=C(C=O)C(OC)=C(OCC3=CC=C(OC(F)(F)F)C=C3)C=C2C1=O</chem>
35	<chem>OC(O)CC2=C(C=O)C(OC)=C(OCC3=CC=C(F)C=C3)C=C2C1=O</chem>
36	<chem>OC(O)CC2=C(C=O)C(OC)=C(OCC3=CC=C(I)C=C3)C=C2C1=O</chem>
37	<chem>OC(O)CC2=C(C=O)C(OC)=C(OCC3=CC=C(Br)C=C3)C=C2C1=O</chem>
38	<chem>OC(O)CC2=C(C=O)C(OC)=C(OCC3=CC=C(Cl)C=C3Cl)C=C2C1=O</chem>
39	<chem>OC(O)CC2=C(C=O)C(OC)=C(OCC3=CC=C(Cl)C(Cl)=C3)C=C2C1=O</chem>

Compound	Smiles
40	<chem>OC(O)CC2=C(C=O)C(OC)=C(OCC3=CC=C(OC4=CC=CC=C4)C=C3)C=C2C1=O</chem>
41	<chem>OC(O)CC2=C(C=O)C(OC)=C(OCC3=CC=C(OC4=CC=C(F)C=C4)C=C3)C=C2C1=O</chem>
42	<chem>OC(O)CC2=C(C=O)C(OC)=C(OCC3=CC=C(C)S3)C=C2C1=O</chem>
43	<chem>OC(O)CC2=C(C=O)C(OC)=C(OCC3=CN=C(C)S3)C=C2C1=O</chem>
44	<chem>OC(O)CC2=C(C=O)C(OC)=C(OCC3=CC(C=CC=C4)=C4C=C3)C=C2C1=O</chem>
45	<chem>OC(O)CC2=C(C=O)C(OC)=C(OCCC3=CC=CC=C3)C=C2C1=O</chem>
46	<chem>OC(O)CC2=C(C=O)C(OC)=C(OCCN3C=CC=C3)C=C2C1=O</chem>
47	<chem>OC(O)CC2=C(C=O)C(OC)=C(OCCCC3=CC=CC=C3)C=C2C1=O</chem>
48	<chem>OC(O)CC2=C(C=O)C(OC)=C(OCCCCC3=CC=C(Cl)C=C3)C=C2C1=O</chem>
49	<chem>OC(O)CC2=C(C=O)C(OC)=C(OCCCCC3=CC=C(F)C=C3)C=C2C1=O</chem>
50	<chem>OC(O)CC2=C(C=O)C(OC)=C(OCCC(C)C)C=C2C1=O</chem>
51	<chem>OC(O)CC2=C(C=O)C(OC)=C(OC/C=C(C)/C)C=C2C1=O</chem>
52	<chem>OC(O)CC2=C(C=O)C(OC)=C(CCCCC)C=C2C1=O</chem>
53	<chem>OC(O)CC2=C(C=O)C(OC)=C(OCCOC)C=C2C1=O</chem>
54	<chem>OC(O)CC2=C(C=O)C(OC)=C(OCCCCF)C=C2C1=O</chem>
55	<chem>OC(O)CC2=C(C=O)C(OC)=C(OCCCC(F)(F)F)C=C2C1=O</chem>
56	<chem>OC(O)CC2=C(C=O)C(OC)=C(OCC3CC3)C=C2C1=O</chem>
57	<chem>OC(O)CC2=C(C=O)C(OC)=C(OCC3CCC3)C=C2C1=O</chem>
58	<chem>OC(O)CC2=C(C=O)C(OC)=C(OCC3CCCC3)C=C2C1=O</chem>
59	<chem>OC(O)CC2=C(C=O)C(OC)=C(OCC3CCCCC3)C=C2C1=O</chem>
60	<chem>OC(O)CC2=C(C=O)C(OC)=C(OCC3CCCCC3)C=C2C1=O</chem>
61	<chem>OC(O)CC2=C(C=O)C(OC)=C(OCC3(C4)CC4C3)C=C2C1=O</chem>